NASA TECHNICAL MEMORANDUM 104225

NASA-TM-104225 19920011240

THE EFFECTS OF UNEVEN FIBER SPACING ON THERMAL RESIDUAL STRESSES IN A UNIDIRECTIONAL SCS-6Ti-15-3 LAMINATE

C. A. Bigelow

March 1992

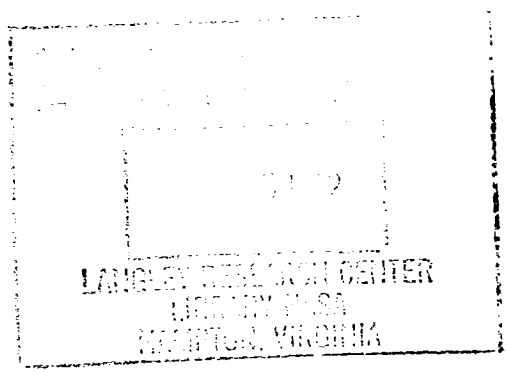

National Aeronautics and
Space Administration

Langley Research Center
Hampton, Virginia 23665

ABSTRACT

High residual stresses develop in SCS-6/Ti-15-3 composites during cooldown from the fabrication temperature; these residual stresses can effect the mechanical and physical properties of the composite. Discrete fiber-matrix finite element models were used to study the residual stresses due to the temperature change during the fabrication process, including the effects of uneven fiber spacing, the free surface, and increased fiber volume fractions.

To accurately model the effects of the free surface, it is only necessary to model one fiber through the thickness. Below the first ply, the analysis predicts stress distributions that are identical to the infinite array predictions.

For uneven fiber spacing less than 0.042 mm in an interior ply, the maximum hoop stress was predicted to occur between fibers within a ply and increased as the fiber spacing decreased. The maximum hoop stress correlated well with the observed radial cracking between fibers. For the case of touching fibers, the analysis predicted tensile radial stresses at the fiber-matrix interface, which could lead to fiber-matrix debonding during the fabrication cooldown. Identical trends were predicted for uneven fiber spacing in surface plies with slightly greater values of maximum stresses.

The analysis predicted matrix yielding to occur upon cooldown when the edge-to-edge fiber spacing was less than or equal to 0.022 mm. The stress distributions predicted for increasing fiber volume fractions were similar to those predicted for decreasing the fiber spacing for two adjacent fibers in a ply.

INTRODUCTION

Metal matrix composites have several inherent properties, such as high stiffness-to-weight ratios and high strength-to-weight ratios, which make them attractive for advanced aerospace applications. These composites also have a higher operating temperature range than polymer matrix composites. However, the

large differences that can exist in the coefficients of thermal expansion of the fiber and the matrix combined with the large temperature change during the fabrication process can lead to problems in these materials. High residual stresses can develop in the composite during cooldown from the fabrication temperature; these residual stresses can affect the mechanical and physical properties of the composite.

The resulting stresses may be large enough to produce matrix cracks and fiber-matrix interfacial debonding, or plastically deform a ductile matrix. For example, the silicon-carbide/titanium composite was found to have a substantial amount of matrix damage in the form of radial cracks in the as-fabricated condition [1]. These microscopic cracks were located at the shortest distance between neighboring fibers in the same row. The amount of cracking was attributed to the effects of fiber spacing; there was consistently more cracking between the more closely spaced fibers within a given row. Additionally, more radial cracking was observed in the surface plies [1].

The present analysis uses discrete fiber-matrix (DFM) models to study thermal residual stresses in a unidirectional composite due to the temperature change during the fabrication process. The DFM models are composed of three-dimensional finite elements. The analysis incorporates temperature-dependent elastic properties in both the fiber and matrix. Temperature-dependent stress-strain behavior of the matrix is also modeled.

The effect of the free surface of the laminate on the thermal residual stresses was studied. A model with a section containing four fibers where the top boundary is a free surface was used. By applying the appropriate boundary conditions, this model represents an infinite sheet with eight plies. Models with one fiber (i.e., two plies) and one quarter of a fiber (i.e., one ply) were used to study the effects of laminate thickness on the thermal residual stresses.

The effects of fiber spacing on thermal residual stresses were studied. An

array of fibers was modeled to accurately account for uneven fiber spacing in interior and surface plies. The effects of fiber spacing on yielding of the matrix during fabrication were also examined. The change in the thermal residual stresses due to increasing the fiber volume fraction was studied and compared with decreasing the fiber spacing of two adjacent fibers.

BACKGROUND

The present work was done to analysis the experimental observations of [1]. Complete details of the material and experimental procedures can be found in [1]. A brief summary of the details pertinent to the present analysis is given here. The alloy Ti-15-3, a shortened designation for Ti-15V-3Cr-3Al-3Sn, is a metastable beta strip alloy [2]. The composite laminates were made by hot-pressing Ti-15-3 foils between unidirectional tapes of silicon-carbide fibers held in place with Ti-6Al-4V wire weaving. The manufacturer's designation for these silicon-carbide fibers is SCS-6. The fiber diameter is 0.14 mm. The composite was an eight-ply unidirectional laminate approximately 2.0 mm thick. The fiber volume fraction was approximately 33 percent.

Polished sections taken from the center of the laminates were examined in both the transverse and longitudinal (parallel to the fiber) directions. The edge-to-edge fiber spacings were measured and correlated to the cracking. Particular emphasis was placed on examination of the outermost and innermost fiber rows of the eight-ply laminate to identify any changes in the amount or distribution of cracks through the specimen thickness. Specimens were examined in the as-fabricated condition and after 10,000 thermal cycles between 300°C and 550°C. Only the thermal cycle due to the thermal cooldown occurring during the fabrication is analyzed in the present work.

As described in [1], the fibers were found to have a fairly wide range in spacing within the same row. The edge-to-edge fiber spacings ranged from 0.0 to 0.160 mm

within the same row, with a large percentage less than 0.020 mm. The mean fiber spacing between fiber rows was .110 mm. Damage was observed in the as-fabricated state as microscopic radial cracks initiating in the fiber-matrix interphase. Specifically, the cracks were located in the outer layers of the carbon-rich coating of the fiber and sometimes extended into the fiber-matrix reaction zone. The results presented in [1] revealed that the most significant cracking occurred during cooldown from consolidation. As previously mentioned, the radial cracks developed where fibers were most closely spaced. A significant difference in the amount of radial cracking was found in the surface and interior fiber rows. Figure 1 presents a histogram of results from [1]. Radial cracking occurred between all fibers spaced up to 0.010 mm for the interior plies and up to 0.020 mm for the surface plies, as shown in Figure 1. The percentage of fibers with cracks decreased as the spacings became wider. No cracks were observed at spacings greater than 0.040 mm for the interior plies or greater than 0.060 mm for the surface plies.

Stress distributions will be presented for the three normal stress components, σ_{rr}, $\sigma_{\theta\theta}$, and σ_{zz}. The radial stress component σ_{rr} controls interfacial or circumferential cracking. The most obvious example of this type of cracking is fiber-matrix debonding. The hoop stress component $\sigma_{\theta\theta}$ controls radial cracking such as was observed in [1]. The axial stress component σ_{zz} governs axial or transverse cracking. Although no damage other than radial cracking was seen in the as-fabricated composite in [1], all three residual stress components will be presented since they may affect the subsequent behavior of the composite.

ANALYTICAL MODELING

For all analyses, discrete fiber-matrix (DFM) models assuming a rectangular array of fibers were used. MSC/NASTRAN [3] was used for the finite element analysis. Three dimensional, eight-noded hexahedral elements were used in the analysis. The ply thickness (0.25 mm), the fiber volume fraction (33%), and the

fiber diameter (0.14 mm) from [1] were used to calculate the spacing for uniformly spaced fibers. From these dimensions, the edge-to-edge fiber spacing for a uniform array is calculated to be 0.052 mm. The uniformly spaced array was used as the reference case.

The temperature was assumed to be uniform throughout the laminate. Since the most significant cracking was observed during cooldown from consolidation, only the thermal cycle occurring during the fabrication process is analyzed in the present work. Thermal residual stresses were calculated assuming a temperature change of -538°C; this temperature change is approximately one half of the melting point of the Ti-15-3 matrix. At absolute temperatures greater than one half the melting point of the matrix, it was assumed that any residual stresses that developed during fabrication of the composite would be relieved due to relaxation [2]. The temperature-dependent constituent elastic properties [4] used are given in Table 1. The matrix properties are given for the as-fabricated material (i.e., no heat treatment). No attempt was made to include any fiber-matrix interface layers or matrix reaction zone in the finite element model. A perfect bond between the fiber and the matrix was assumed. The tabulated values for the temperature-dependent matrix stress-strain curves [4] are given in Table 2. The fiber was assumed to remain elastic. All analyses assumed material nonlinearity to allow matrix yielding. Yielding of the matrix was predicted by comparing the von Mises equivalent stress to the room temperature yield stress (689.48 MPa [4]). When the von Mises equivalent stress was greater than or equal to the yield stress, yielding of the matrix was assumed. The von Mises equivalent stress σ_{vm} is defined as follows:

$$\sigma_{vm} = \sqrt{\sigma_x^2 + \sigma_y^2 + \sigma_z^2 - \sigma_x\sigma_y - \sigma_y\sigma_z - \sigma_z\sigma_x + 3(\tau_{xy}^2 + \tau_{yz}^2 + \tau_{zx}^2)}$$

Laminate Thickness Models

Four DFM models were used to examine the effect of laminate thickness on the thermal residual stresses due to the fabrication process. All DFM models were defined assuming one layer of fibers in each ply of the laminate. A DFM model with one quarter of a fiber and the surrounding matrix was used as the basic building block. Figure 2(a) shows the dimensions of the unit cell for the fiber volume fraction of 33%. The model shown in Figure 2(a) was used with the appropriate boundary conditions to represent a single fiber in an infinite array of fibers and to represent a unidirectional, one-ply lamina. For the single fiber in an infinite array, compatibility with adjacent unit cells was enforced on each face of the model by constraining all normal displacements to be equal. For the one-ply lamina, the top surface (y = 0.125 mm) was modeled as a free boundary (i.e., no constraints were used) and compatibility with adjacent unit cells was enforced on each of the other faces of the model by constraining all normal displacements to be equal. A model with one fiber (Figure 2(b)) was used represent a laminate with two plies. A model containing four fibers (Figure 2(c)) was used to model a unidirectional composite with eight plies. For reference, the fibers are labeled from 1 to 4. For both Figures 2(b) and 2(c), the top surface was modeled as a free boundary (i.e., no constraints were used) and compatibility with adjacent unit cells was enforced on each of the other faces of the model by constraining the normal displacement to be equal.

Fiber Spacing Models

Two different fiber spacing models were developed. The first model represented an infinite array of fibers with uneven fiber spacing. This model was designed to represent the interior plies. The second model represented the same fiber spacings in a surface ply.

Infinite Array Model. - A model with twelve fibers is shown in Figure 3. For

reference, the fibers are labeled from 1 to 12. The array of fibers and the model dimensions used for the reference case of uniform spacing ($S_1 = S_2 = 0.052$ mm) are shown in the figure. To model different spacings, fibers 6 and 7 were shifted towards each other by equal but varying amounts. The values of S_1 and S_2 used are given in Table 3. Consistent with the experimental observations [1], the distance between fibers in each ply t_p was kept constant ($t_p = .110$ mm). By shifting fibers 6 and 7 towards each other, the edge-to-edge fiber spacing was varied from .078 mm to 0.0 mm. S_1 varied form 0.052 mm to 0.0 mm while S_2 varied from 0.052 mm to 0.078 mm. For clarity, stress distributions will be presented only for the area located between Fibers 6 and 7 indicated by the dashed line in Figure 3.

Surface Ply Model. - An array of eight fibers was used to model uneven fiber spacing in the surface ply. Figure 4 shows the array of fibers and model dimensions used for the reference case of uniform spacing. The fibers are labeled from 1 to 8, and as before, Fibers 6 and 7, now in the surface ply, were shifted by varying amounts to model different fiber spacings. The top surface was modeled as a free boundary (i.e., no constraints were imposed). The normal displacements on each of the other faces were constrained to be equal.

Models for Increasing Fiber Volume Fraction

To model increasing v_f, only one quarter of the fiber and the surrounding matrix were modeled (Figure 2(a)). The distance between plies was held constant and the spacing between the fibers was decreased from the reference case, $S_1 = 0.052$ mm. In the fabrication of metal matrix composites using the foil-fiber-foil technique, constant thickness foils are usually used and one method of increasing the fiber volume is decreasing the fiber spacing. Six values of the fiber volume fraction were used. Starting with the reference value of v_f of 33%, it was assumed that only increasing values of v_f would be of interest. For the fiber spacings of 0.0, 0.012, 0.022, 0.032, 0.042, and 0.052 mm, the corresponding values of v_f are 44, 41,

38, 36, 34, and 33%.

RESULTS AND DISCUSSION

The analytical results are presented as stress contour plots for the matrix only. The calculated fiber stresses (σ_{rr}, $\sigma_{\theta\theta}$, and σ_{zz}) due to the thermal load were compressive, and thus, are not presented here. In the stress contour plots, the areas represented by the fibers are shown as blanks. All matrix stresses are plotted with respect to a cylindrical coordinate system, as shown in Figure 2, with the origin at the center of the fiber.

Free Surface Effects

The thermal residual stresses in the matrix due to the fabrication process ($\Delta T = -538^{\circ}C$) were determined for the models defined in Figure 2. All six stress components predicted for the eight-ply model (Figure 2(c)) were identical around fibers 2 through 4 and the stresses predicted around fibers 2 through 4 of the eight-ply model were identical to the stresses predicted for the infinite array model. The stresses predicted around the surface fiber (fiber 1) were identical to the stresses predicted for the two-ply model (Figure 2(b)). The stresses predicted for the upper half of the two-ply model (Figure 2(c)) were identical to those predicted for the one-ply model. However, the stresses predicted for the lower half of the two-ply model (Figure 2(c)) were not identical to the stresses predicted for the infinite array. The stress distributions were very similar, but not identical. Thus, to account for the free surface in a unidirectional composite, it is necessary to model a two-ply laminate (a single fiber), as shown in Figure 2(c).

To quantify the effect of the free surface, the stress contours for the two-ply model and the infinite array model will be compared in detail. The σ_{rr} stresses in the matrix for the two-ply and infinite array models are presented in Figures 5 and 6, respectively. The radial stresses in the two-ply model near the upper surface of the model are smaller than in the infinite array model. This difference is due to the

free surface boundary condition used in the two-ply model. As the centerline of the fiber ($\theta = 0^o$) is approached, the two solution become nearly identical. The presence of the free surface relieves the thermal residual stress in the surface ply. Since the compressive σ_{rr} thermal residual stress would have to be overcome by a mechanical load to cause interfacial failure, surface plies could experience interfacial failure earlier in the loading history.

The $\sigma_{\theta\theta}$ stresses in the matrix for the two-ply and infinite array models are presented in Figures 7 and 8, respectively. The $\sigma_{\theta\theta}$ stresses are tensile throughout the matrix for both models. The $\sigma_{\theta\theta}$ stresses are, in general, larger for the two-ply model. Along the x-axis (where the fibers are closest together) the stress is slightly greater (1%) for the two-ply model. For these two cases with uniform fiber spacing, the maximum value of the $\sigma_{\theta\theta}$ stress is not found at $\theta = 0^o$. For the two-ply model (Figure 7), the peak value of $\sigma_{\theta\theta}$ occurs in the fiber-matrix interface region, over a range of θ from 90^o to approximately 45^o. For the infinite array case (Figure 8), the peak value of $\sigma_{\theta\theta}$ also occurs at the fiber-matrix interface near $\theta = 45^o$. These predictions seem to contradict the experimental observations that radial cracking always occurred between fibers in a ply (i.e., at $\theta = 0^o$). However, no cracking was observed for the fiber spacing used in these models ($S_1 = 0.052$ mm); thus, the maximum stress was obviously not large enough to cause cracking at this spacing. Other fiber spacings will be discussed in a later section.

The σ_{zz} stresses in the matrix for the two-ply and infinite array models are presented in Figures 9 and 10, respectively. For $\theta \leq 30^o$, the stresses are very similar for the two models, although slightly larger for the two-ply model. Near the upper surface, the two-ply model predicts σ_{zz} stresses that are 2 to 8% greater than the infinite array model and the maximum value of the σ_{zz} stress in the two-ply model is predicted at the free surface. This seems to contradict intuition; a free surface should cause a lower stress than a plane that is constrained. However, in

this case, intuition is misleading. For the infinite array model, the σ_{zz} stress is maximum along a radial line at approximately 45° and above this line, the σ_{zz} stress is nearly constant for the infinite array. Below this 45° line, the σ_{zz} stress decreases in both models. The constraint provided by the fiber causes the σ_{zz} stress to decrease. In the infinite array model, the presence of another fiber above would have the same effect on the σ_{zz} stresses. In the two-ply model, there is no fiber above, thus, no constraining effect and the σ_{zz} stresses are greater with a free surface.

Effects of Uneven Fiber Spacing

Interior Plies

The σ_{rr}, $\sigma_{\theta\theta}$, and σ_{zz} stress contours for the edge-to-edge fiber spacings using the model shown in Figure 3 are presented in Figures 11, 12 and 13, respectively. In this model, Fibers 6 and 7 are shifted by varying amounts to represent uneven fiber spacing within an interior ply. The stresses around each fiber are defined with respect to a cylindrical coordinate system whose origin is located at the center of that fiber. As indicated in Figure 3, stress contours are shown only for part of the area between Fibers 6 and 7. Thus, stress contours are presented for S_1 ranging from 0.052 mm to 0.0 mm. This was done for clarity. Stress values for the larger fiber spacings, S_2 ranging from 0.052 mm to 0.078 mm, are presented in a later section.

The σ_{rr} stress contours for decreasing edge-to-edge fiber spacings are presented in Figure 11. Note that in this and subsequent figures, different stress levels are used in each contour plot. Figure 11(a) presents the σ_{rr} stress contours for the reference case of uniform fiber spacing ($S_1 = S_2 = 0.052$ mm). As S_1, the edge-to-edge fiber spacing of Fibers 6 and 7, decreases, the maximum compressive radial stresses between the two fibers ($\theta = 0^0$) becomes more compressive. The σ_{rr} stress at the fiber-matrix interface near $\theta = 45^0$ decreases slightly with decreasing

fiber spacing. However, the stresses are still compressive for all spacings greater than 0.0 mm, indicating that no interfacial failure would occur due to the thermal cycle. However, for the case of touching fibers (Fig. 11(f)), the radial stresses are tensile on part of the fiber-matrix interface near $\theta = 45^{\circ}$. Depending upon the strength of the interface region, the closer fiber spacing could lead to earlier failures of the fiber-matrix interface when mechanical loadings were applied. If the interface were weak enough, the interface could fail upon thermal cooldown if fibers were touching.

The $\sigma_{\theta\theta}$ stress contours for decreasing edge-to-edge fiber spacings are presented in Figure 12. Figure 12(a) presents the $\sigma_{\theta\theta}$ stress contours for the reference case of uniform fiber spacing. The $\sigma_{\theta\theta}$ stresses are tensile throughout the matrix for all edge-to-edge fiber spacings. For $S_1 \geq 0.042$ mm, the maximum $\sigma_{\theta\theta}$ stresses occur in the fiber-matrix interface region near the top of the fiber, at $\theta = 90^{0}$ and between each fiber at $\theta = 0^{\circ}$, there is a zone of relatively large $\sigma_{\theta\theta}$ stresses connecting each fiber. For $S_1 \geq 0.42$ mm (Figs. 12(a) and (b)), the stress at $\theta = 0^{\circ}$ is within 10% of the maximum. As S_1 decreases, the maximum stress is now predicted between the two fibers at $\theta = 0^{\circ}$. For spacings less than 0.42 mm (Figs. 12(c), (d) and (e)), the $\sigma_{\theta\theta}$ stress is maximum at $\theta = 0^{\circ}$. For a spacing of zero (Fig. 12(f)), the maximum value of $\sigma_{\theta\theta}$ does not occur exactly at $\theta = 0^{\circ}$ since there is no matrix material there, but in the matrix material slightly above the point where the fibers touch. These predictions seem to contradict the experimental observations that radial cracking always occurred between fibers in a ply (i.e., at $\theta = 0^{0}$). However, no cracking was observed for the fiber spacings greater than 0.040 mm (see Fig. 1 or [1]); thus, the maximum stress was obviously not large enough to cause cracking for spacings greater than 0.040 mm. For spacings less than 0.042 mm, the analysis predicted that the maximum hoop stress was between the fibers and increased as the fiber spacing decreased. The calculated value of $\sigma_{\theta\theta}$ at $\theta = 0^{\circ}$

increased by 55% over the range of fiber spacing analyzed. Thus, the predicted maximum hoop stress correlates well with the observed cracking.

The σ_{zz} stress contours for decreasing edge-to-edge fiber spacings are presented in Figure 13. Figure 13(a) presents the σ_{zz} stress contours for the reference case of uniform fiber spacing. For all spacings the maximum σ_{zz} stresses occur at $\theta = 45^{0}$. As S_1 decreases, the magnitude of the maximum σ_{zz} stress increases by 22%. The minimum value of the σ_{zz} stress occurs between the most closely spaced fibers within a ply ($\theta = 0^{0}$), and as the fiber spacing decreases, the minimum value of σ_{zz} decreases.

Surface Ply

The σ_{rr}, $\sigma_{\theta\theta}$, and σ_{zz} stress contours for various edge-to-edge fiber spacings in a surface ply (Figure 4) were also predicted. As before, Fibers 6 and 7 are shifted by varying amounts to represent uneven fiber spacing. In this case, the upper surface of the model represents a free surface. All stress components were calculated with respect to the cylindrical coordinate system as defined in Figure 2. The stresses around each fiber are defined with respect to a cylindrical coordinate system whose origin is located at the center of that fiber.

The trends in the σ_{rr} stress contours for decreasing edge-to-edge fiber spacings in the surface ply were identical to those shown previously for the interior plies. The maximum (compressive) values of the radial stress for the surface and interior plies are presented in Figure 14. As shown, the predicted trends are identical for the surface and interior plies and the maximum σ_{rr} stresses were elevated in the surface ply slightly (less than 5%) for S_1 less than 0.032 mm.

The trends in the $\sigma_{\theta\theta}$ stress contours for decreasing edge-to-edge fiber spacings in the surface ply were similar to those shown previously for the interior plies. The maximum values of the hoop stress at $\theta = 0^{o}$ for the surface and interior plies are presented in Figure 15. As shown, the predicted trends are similar for the surface

and interior plies. Decreasing the fiber spacing from the reference case (S_1 = 0.052 mm) to the case of touching fibers (S_1 = 0.0 mm) produced a 88% increase in the maximum $\sigma_{\theta\theta}$ stress. For spacings greater than 0.042 mm, the maximum $\sigma_{\theta\theta}$ stress is predicted in the interior ply; for spacing less than 0.042 mm, the maximum $\sigma_{\theta\theta}$ stress is predicted in the surface ply. However, for all spacings, the free surface changed the maximum $\sigma_{\theta\theta}$ stress by less than 5%. Obviously, the predicted effect of the free surface is not large and, thus, may not account for the increase in cracking observed in the surface plies.

The trends in the σ_{zz} stress contours for decreasing edge-to-edge fiber spacings in the surface ply were similar to those shown previously for the interior plies. The maximum values of the axial stress for the surface and interior plies are presented in Figure 16. As shown, the predicted trends are similar for the surface and interior plies. Decreasing the fiber spacing from the reference case (S_1 = 0.052 mm) to the case of touching fibers (S_1 = 0.0 mm) produced a 16% increase in the maximum σ_{zz} stress. For all spacings, the free surface increased the maximum σ_{zz} stress by less than 5%.

Matrix Yielding

The von Mises equivalent stress was calculated to determine matrix yielding. No yielding was predicted for spacings greater than or equal to 0.032 mm. Figure 17 shows the matrix yield patterns for S_1 = 0.022, 0.012 and 0.0 mm for the interior plies. With the closer fiber spacings, the analysis predicts the matrix will yield in the area between the fibers due to the thermal cooldown in the fabrication process. The yield patterns predicted for the surface ply were nearly identical to those predicted for the interior plies and, thus, are not shown.

Effects of Increasing Fiber Volume Fraction

Increasing the fiber volume fraction, which is equivalent to decreasing the fiber spacing for all fibers in the composite, had the same effects as decreasing the

fiber spacing between two adjacent fibers only. The σ_{rr} stresses in the matrix at the fiber matrix interface are shown in Figure 18. As the fiber volume fraction increases, the stresses between the fibers become more compressive. The stress near the top of the fiber ($\theta = 90^0$) decreases slightly in magnitude with increasing v_f. However, the stresses are still compressive for all values of v_f except for v_f = 44% (touching fibers), indicating that no interfacial failure would occur due to the thermal cycle. For the case of touching fibers, the radial stresses are tensile on part of the fiber-matrix interface, from $\theta = 32^0$ to 58^0. Depending upon the strength of the interface region, the closer fiber spacing could lead to fiber-matrix debonding during the fabrication process and earlier failures of the fiber-matrix interface when mechanical loadings are applied.

The $\sigma_{\theta\theta}$ stress values predicted between the fibers within a ply for increasing fiber volume fractions are shown in Figure 19. The $\sigma_{\theta\theta}$ stresses are tensile throughout the matrix for all fiber volume fractions. For $v_f \leq 34\%$, the maximum stresses occur in the fiber-matrix interface region near the top of the fiber, at $\theta = 90^0$ and there is a zone of relatively large $\sigma_{\theta\theta}$ stresses between each fiber at $\theta = 0^0$. For $v_f \leq 34\%$, the stress at $\theta = 0^0$ is within 11% of the maximum. As v_f increases, the maximum stress is now predicted between two fibers ($\theta = 0^0$). For v_f greater than 34%, the $\sigma_{\theta\theta}$ stress is maximum at $\theta = 0^0$. For v_f = 44% (touching fibers), the maximum value of $\sigma_{\theta\theta}$ does not occur at $\theta = 0^0$, but slightly above the point where the fibers touch. The values of $\sigma_{\theta\theta}$ at $\theta = 0^0$ for increasing v_f (solid circles) are shown in Figure 19. The values of $\sigma_{\theta\theta}$ predicted for the decreasing fiber spacings for the interior (open circles) and surface plies (open squares) are also shown in Figure 19. For comparison, all stresses are plotted as a function of the fiber spacing and the appropriate fiber volume fractions are shown in parentheses. Less than a 5% difference was predicted for the three cases.

The trend in the σ_{zz} stresses predicted for increasing fiber volume fractions

was similar to that predicted for the decreasing fiber spacings. For all values of v_f the maximum σ_{zz} stresses occur at $\theta = 45^o$; as the fiber volume fraction increases, the magnitude of the maximum σ_{zz} stress increased. However, the increase in the maximum σ_{zz} stresses predicted for the increasing fiber volume fractions is significantly larger than that predicted for the decreasing fiber spacings. For comparison, the maximum σ_{zz} stresses predicted for increasing fiber volume fraction (solid circles) and for the interior (open circles) and surface plies (open squares) are shown in Figure 20. All stresses are plotted as a function of the fiber spacing and the appropriate fiber volume fractions are shown in parentheses. The maximum value of σ_{zz} changed by 26% due to increasing the fiber volume fraction, compared to a change of 16% for the decreased fiber spacing in both interior and surface plies).

Material manufacturers may desire an increased fiber volume fraction to obtain higher strength composites. These results, however, indicate that an increasing v_f may lead to problems; damage may occur during the fabrication process if the fibers are too closely spaced. Even if no damage occurs during the processing, the thermal residual stresses developed may significantly affect the subsequent mechanical behavior of the composite.

CONCLUSIONS

High residual stresses develop in SCS-6/Ti-15-3 composites during cooldown from the fabrication temperature; these residual stresses can affect the mechanical and physical properties of the composite. Discrete fiber-matrix (DFM) finite element models were used to study the residual stresses due to the temperature change during the fabrication process. The analysis incorporated temperature-dependent elastic properties in both the fiber and matrix. Temperature-dependent stress-strain behavior of the matrix was also modeled.

The following conclusions were made for thermal loading of a unidirectional

SCS-6/Ti-15-3 composite:

To accurately model the effects of the free surface, it is only necessary to model one fiber through the thickness. Below the first ply, the analysis predicts results that are identical to the infinite array results. The free surface slightly reduced the radial stresses at the fiber-matrix interface which could lead to fiber-matrix debonding at lower load levels upon subsequent mechanical loading.

For uneven fiber spacing in an interior ply less than 0.042 mm, the maximum hoop stress was predicted to occur between fibers within a ply and increased as the fiber spacing decreased. The maximum hoop stress between fibers within a ply correlated well with the observed radial cracking between fibers for interior plies [1]. For the case of touching fibers, the analysis predicted tensile radial stresses at the fiber-matrix interface. Depending on the fiber-matrix interface strength, fiber-matrix debonding could occur during the fabrication cooldown. For all spacings the maximum σ_{zz} stress occurred at $\theta = 45^0$ and increased as the fiber spacing decreased. Identical trends were predicted for uneven fiber spacing in surface plies with slightly greater values of peak stresses.

The analysis predicted matrix yielding to occur upon cooldown when the edge-to-edge fiber spacing was less than or equal to 0.022 mm. A small area of matrix material between the most closely spaced fibers was predicted to yield.

Increasing fiber volume fractions were modeled using unit cells with decreasing edge-to-edge fiber spacing, while the ply-to-ply fiber spacing was held constant. The results predicted for increasing fiber volume fractions were similar to the results predicted for decreasing the fiber spacing between two adjacent fibers in a ply. A greater increase in the axial stress component was predicted for increasing fiber volume fraction than for decreasing fiber spacing between adjacent fibers. The results indicate that matrix cracking and fiber-matrix debonding are more likely to occur during processing for laminates with higher fiber volume fractions.

The results presented here indicate that significant increases in stresses may occur during the fabrication process when the fibers are too closely spaced. Even if no damage occurs during the processing, the thermal residual stresses developed may affect the subsequent mechanical behavior of the composite and, thus, these effects should be understood and quantified.

REFERENCES

1. MacKay, Rebecca A.: Effect of Fiber Spacing on Interfacial Damage in a Metal Matrix Composite. Scripta METALLURGICA et MATERIALA, Vol. 24, pp. 167-172, 1990.

2. Dieter, G. E.: Mechanical Metallurgy. 2nd Ed., McGraw-Hill, New York, 1976, pp. 451-489.

3. MSC/NASTRAN, Version 6.6, MacNeal-Schwendler Corporation, 1991.

4. Johnson, W. S.; Lubowinski, S. J.; and Highsmith, A. L.: Mechanical Characterization of Unnotched SCS /Ti-15-3 Metal Matrix Composites at Room Temperature. Thermal and Mechanical Behavior of Metal Matrix and Ceramic Matrix Composites, ASTM STP 1080, J. M. Kennedy, H. H. Moeller, and W. S. Johnson, Eds., American Society for Testing and Materials, Philadelphia, 1990, pp. 193-218.

Table 1 - Temperature-Dependent Constituent Properties For SCS-6/Ti-15-3 [4]

Elastic Properties for Ti-15-3 Matrix (as-fabricated)

Temp	E	ν	α
°C	Pa		mm/mm/°C
21.11	9.239E10	.36	8.208E-6
204.44	9.239E10	.36	8.946E-6
426.67	8.481E10	.36	9.504E-6
537.78	5.861E10	.36	9.756E-6

Elastic Properties for SCS-6 Fiber

Temp	E	ν	α
°C	Pa		mm/mm/°C
21.11	3.93E11	.25	3.564E-6
93.33	3.90E11	.25	3.564E-6
204.44	3.86E11	.25	3.618E-6
315.56	3.82E11	.25	3.726E-6
426.67	3.78E11	.25	3.906E-6
537.78	3.74E11	.25	4.068E-6
648.89	3.70E11	.25	4.266E-6
760.00	3.65E11	.25	4.410E-6
871.11	3.61E11	.25	4.572E-6
1093.30	3.54E11	.25	

Table 2 - Tabulated Data for Ti-15-3 Matrix Stress-Strain Curves (as-fabricated)

Temp °C	Strain mm/mm	Stress Pa
21.11	0.0	0.0
	0.0076	6.8948E8
	0.0082	7.4119E8
	0.0088	7.8428E8
	0.0094	8.2737E8
	0.0098	8.4461E8
	0.0106	8.7908E8
	0.0113	8.9632E8
	0.0118	9.0494E8
	0.0124	9.1356E8
	0.0132	9.2217E8
	0.0146	9.3079E8
	0.0168	9.3941E8
	0.0208	9.4803E8
537.78	0.0	0.0
	0.0071	4.1385E8
	0.0171	4.4816E8
	0.0321	5.0000E8

Table 3 - Fiber Spacings

CASE	S_1 (mm)	S_2 (mm)
Uniform	0.052	0.052
Spacing 1	0.042	0.057
Spacing 2	0.032	0.062
Spacing 3	0.022	0.067
Spacing 4	0.012	0.072
Touching	0.0	0.078

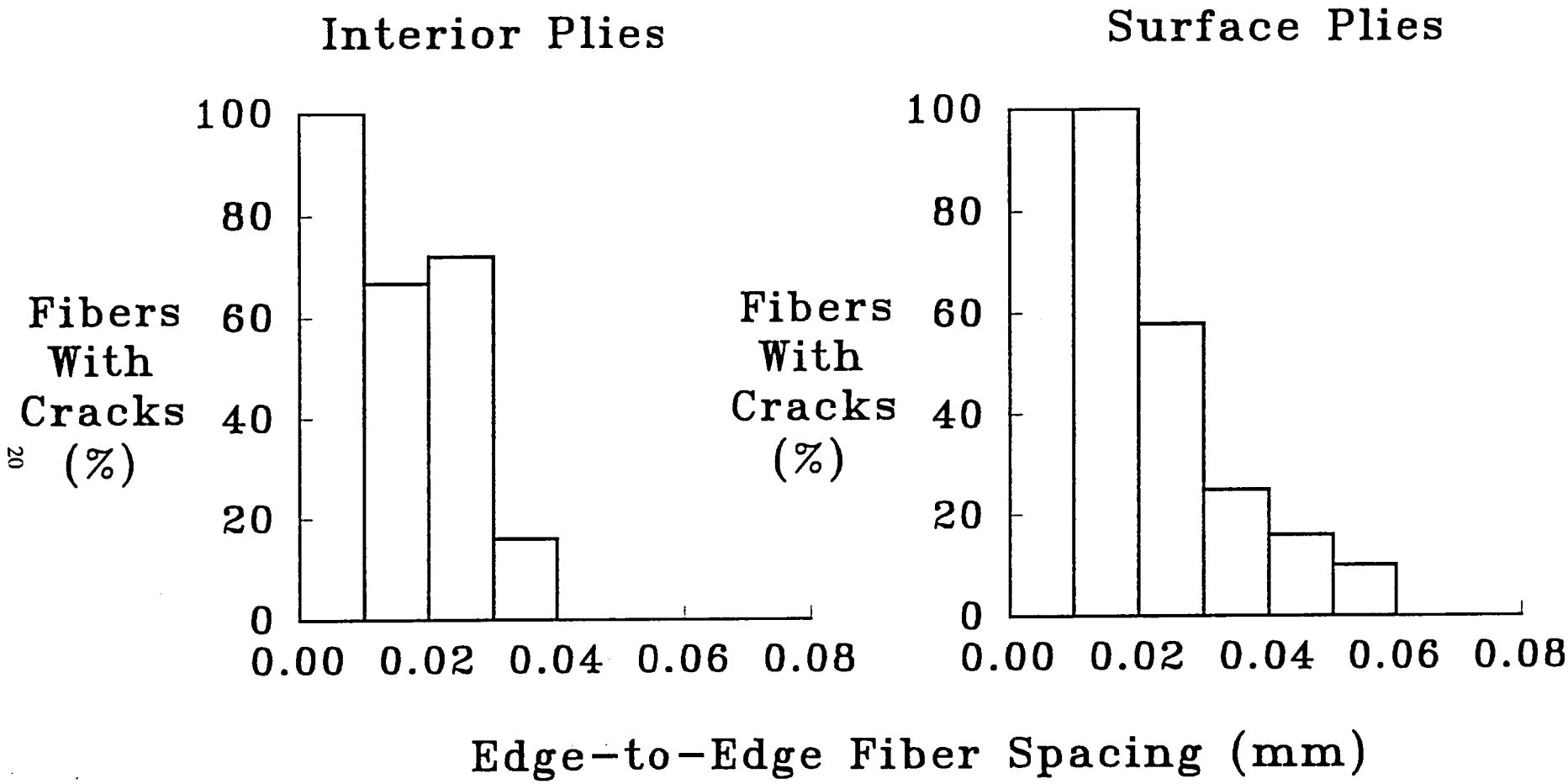

Figure 1. - Histogram of measured percent of fibers with radial cracks as a function of the edge-to-edge fibers spacing in unidirectional SCS-6/Ti-15-3, v_f = 33%. Data from [1].

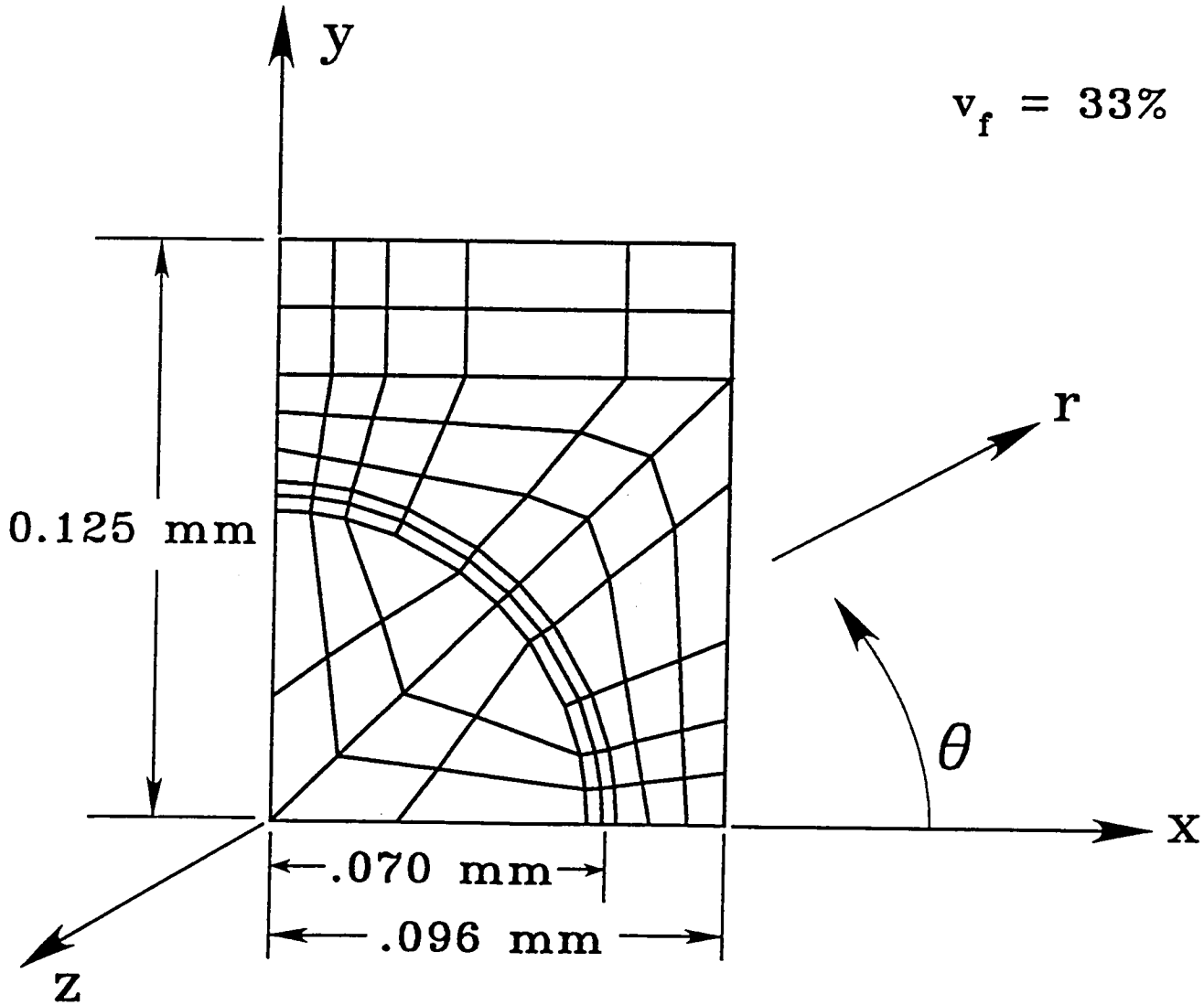

(a) Unit cell dimensions and coordinate system for the infinite array model.

Figure 2. - Configurations and finite element meshes for laminate thickness models.

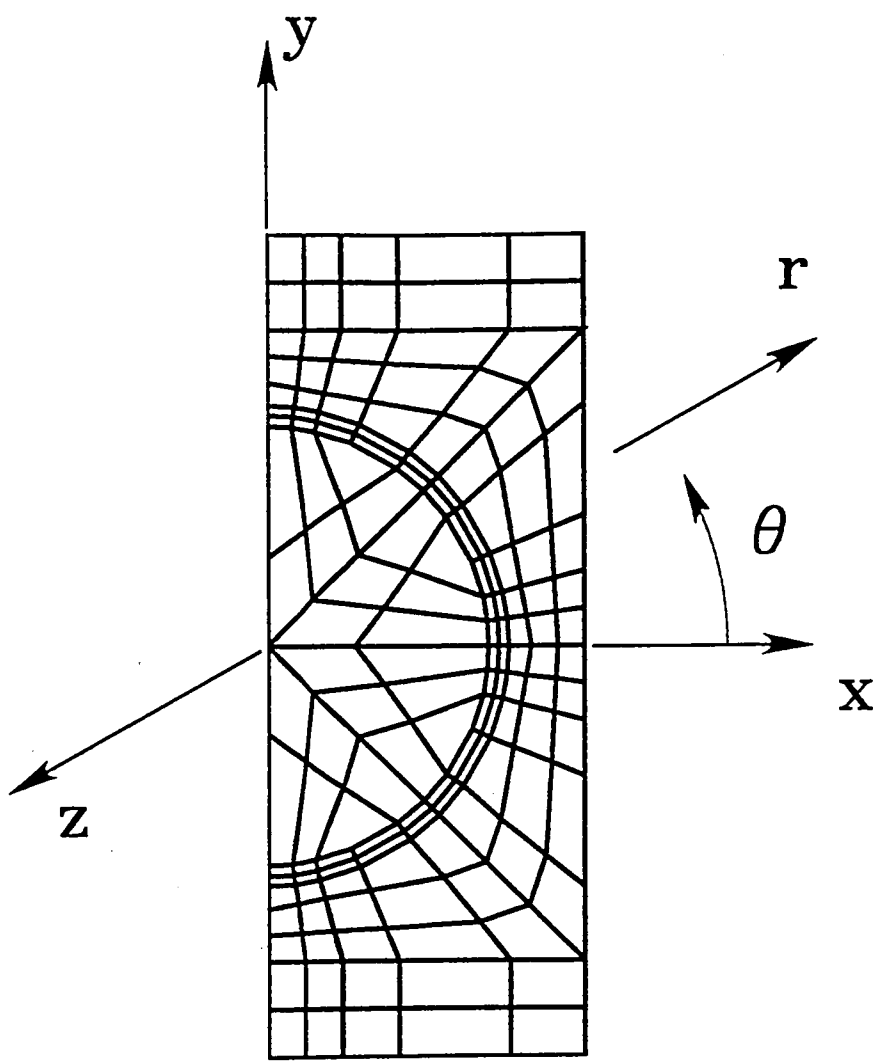

(b) Two-ply finite element model.

Figure 2. - Continued

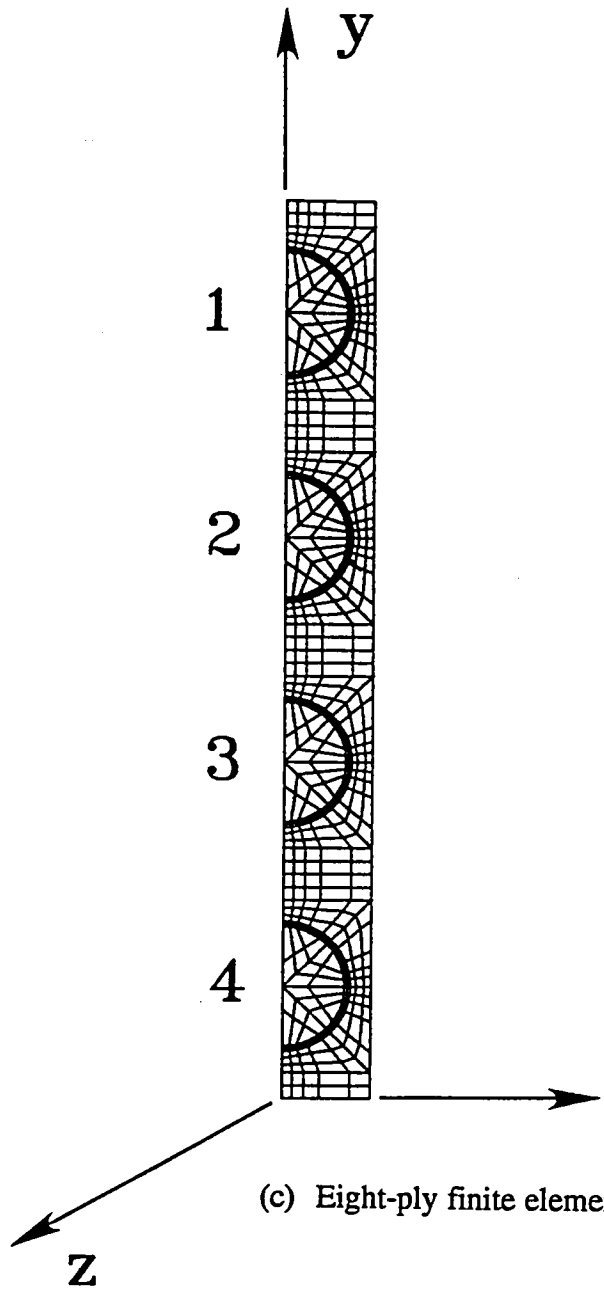

(c) Eight-ply finite element model.

Figure 2. - Continued

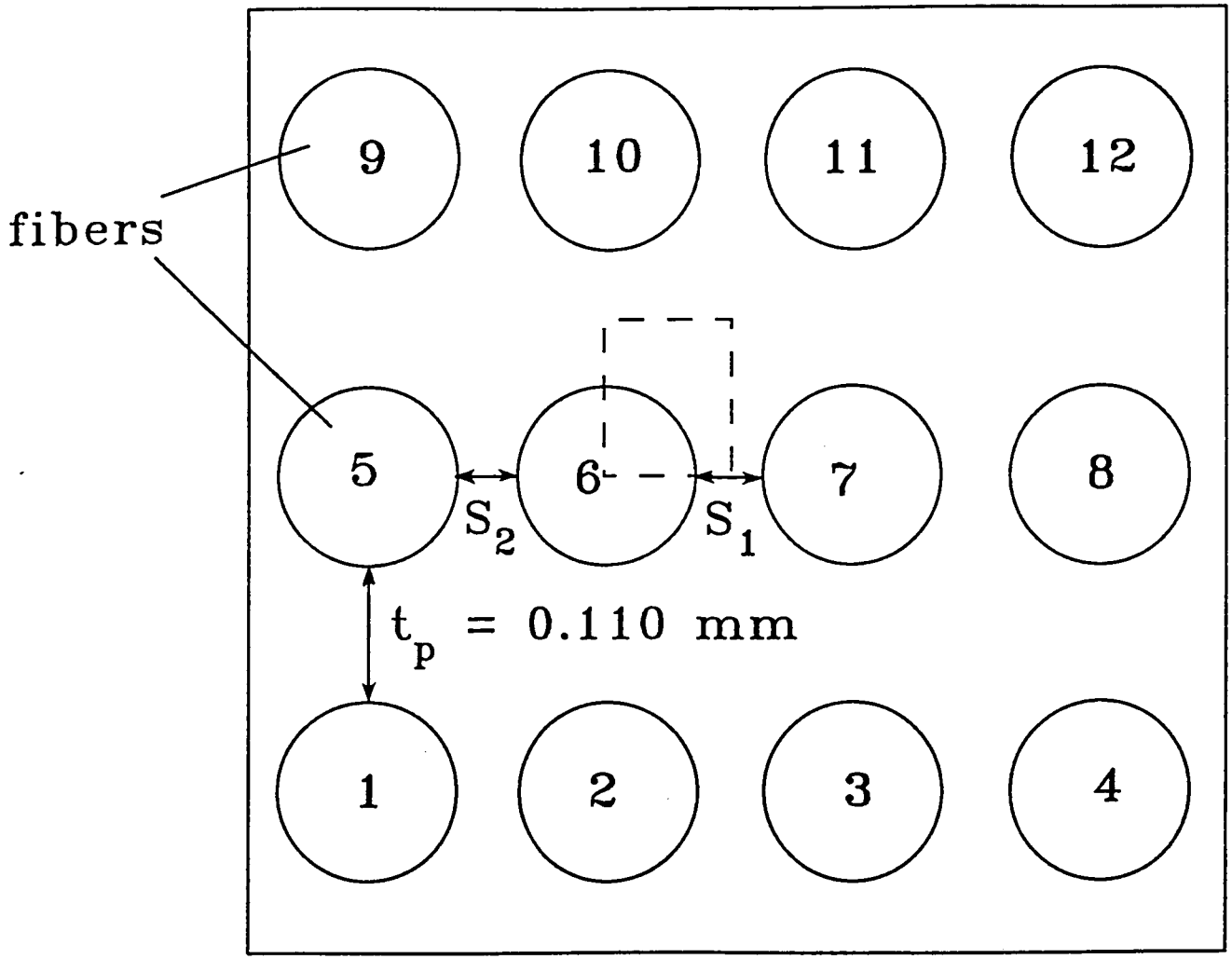

Figure 3. - Fiber spacing model for interior plies.

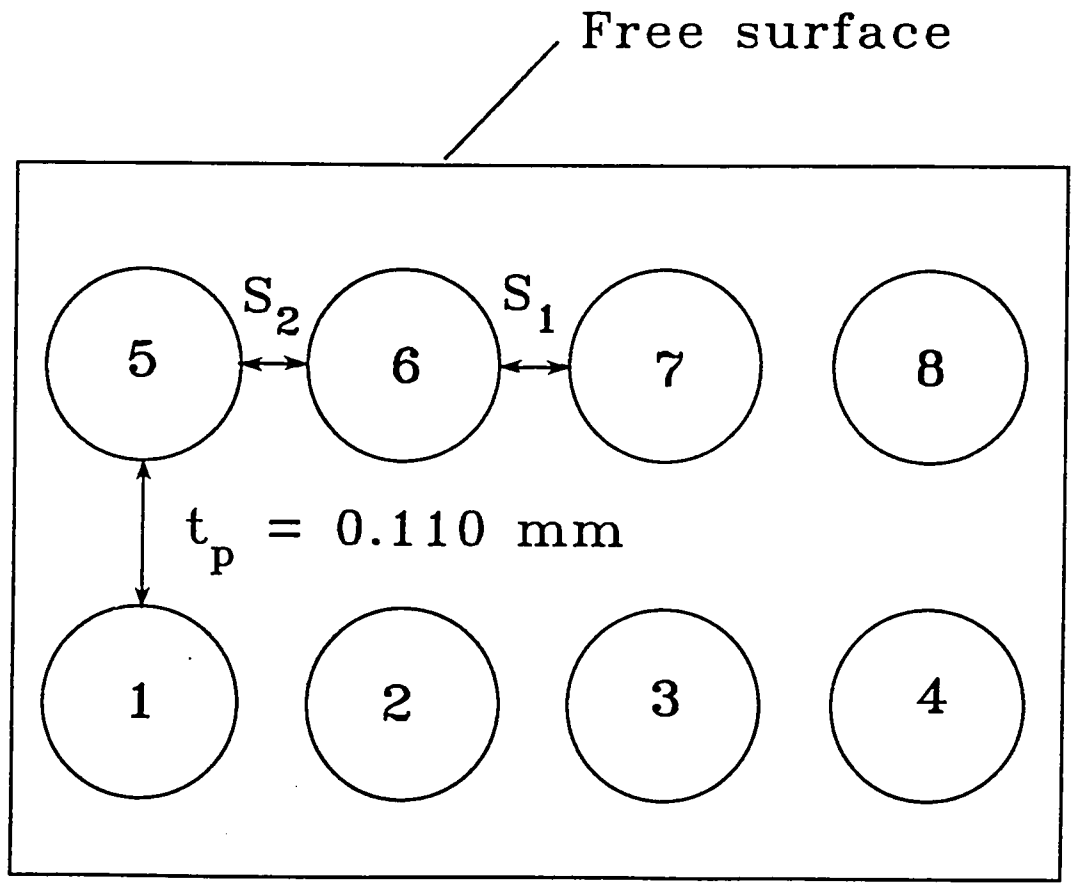

Figure 4. - Fiber spacing model for surface ply.

Level	Stress (MPa)
A	63.5
B	41.1
C	18.6
D	-3.9
E	-26.4
F	-48.9
G	-71.4
H	-93.9
I	-116
J	-139
K	-161
L	-183
M	-206
N	-229
O	-251

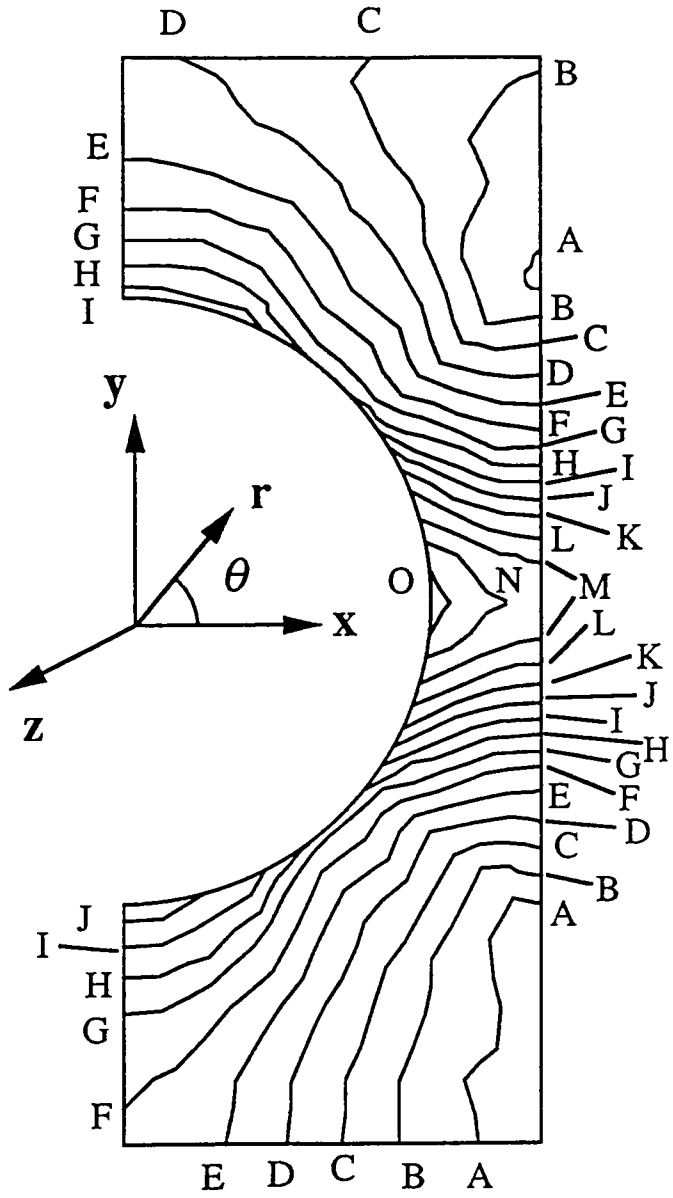

Figure 5. - Matrix σ_{rr} stress contours for two-ply model. Unidirectional SCS-6/Ti-15-3, v_f = 33%, ΔT = -538°C.

Level	Stress (MPa)
A	63.5
B	41.1
C	18.6
D	-3.9
E	-26.4
F	-48.9
G	-71.4
H	-93.9
I	-116
J	-139
K	-161
L	-183
M	-206
N	-229
O	-251

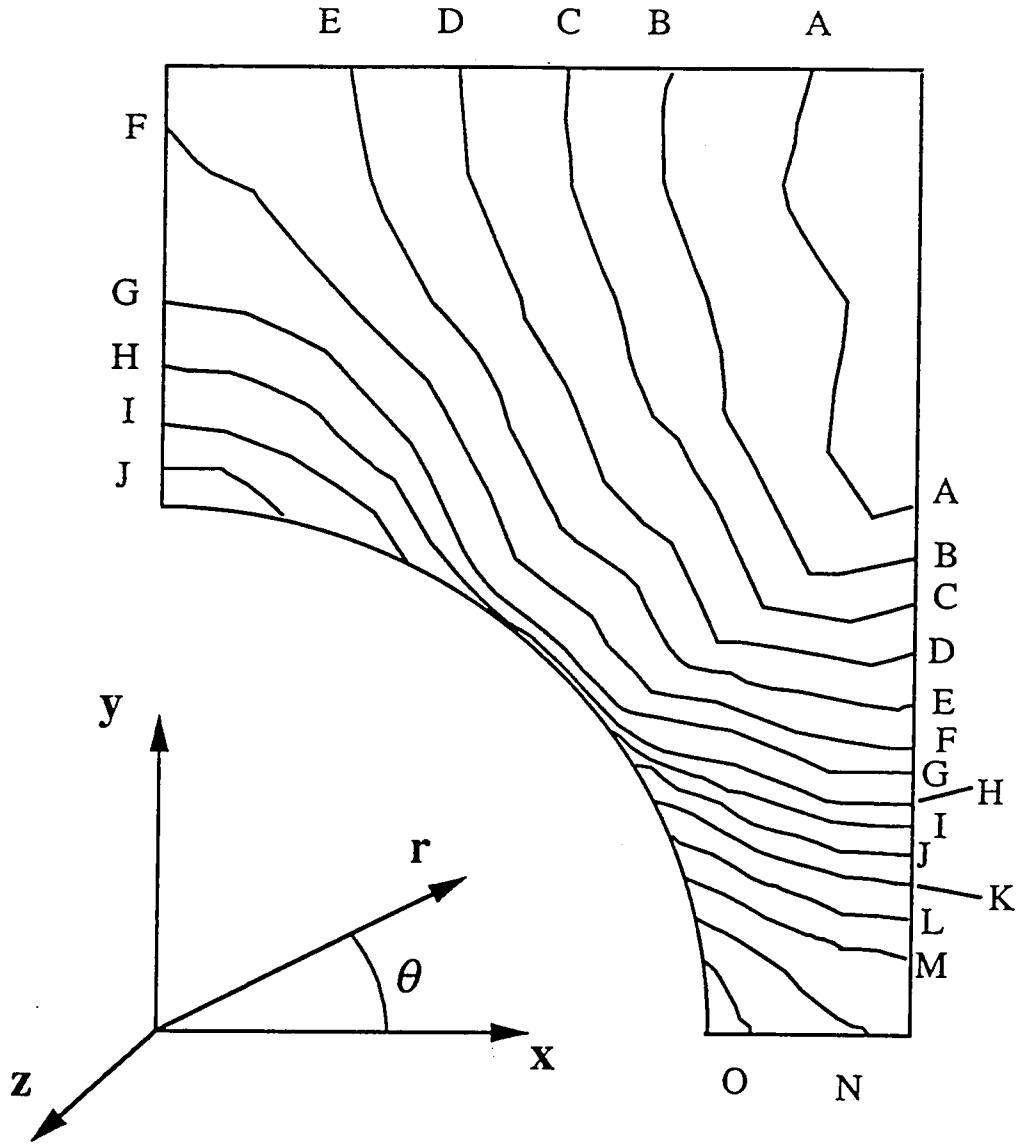

Figure 6. - Matrix σ_{rr} stress contours for infinite array model. Unidirectional SCS-6/Ti-15-3, v_f = 33%, ΔT = -538°C.

Level	Stress (MPa)
A	312
B	296
C	278
D	262
E	245
F	228
G	212
H	195
I	178
J	161
K	144
L	128
M	111
N	94.0
O	77.2

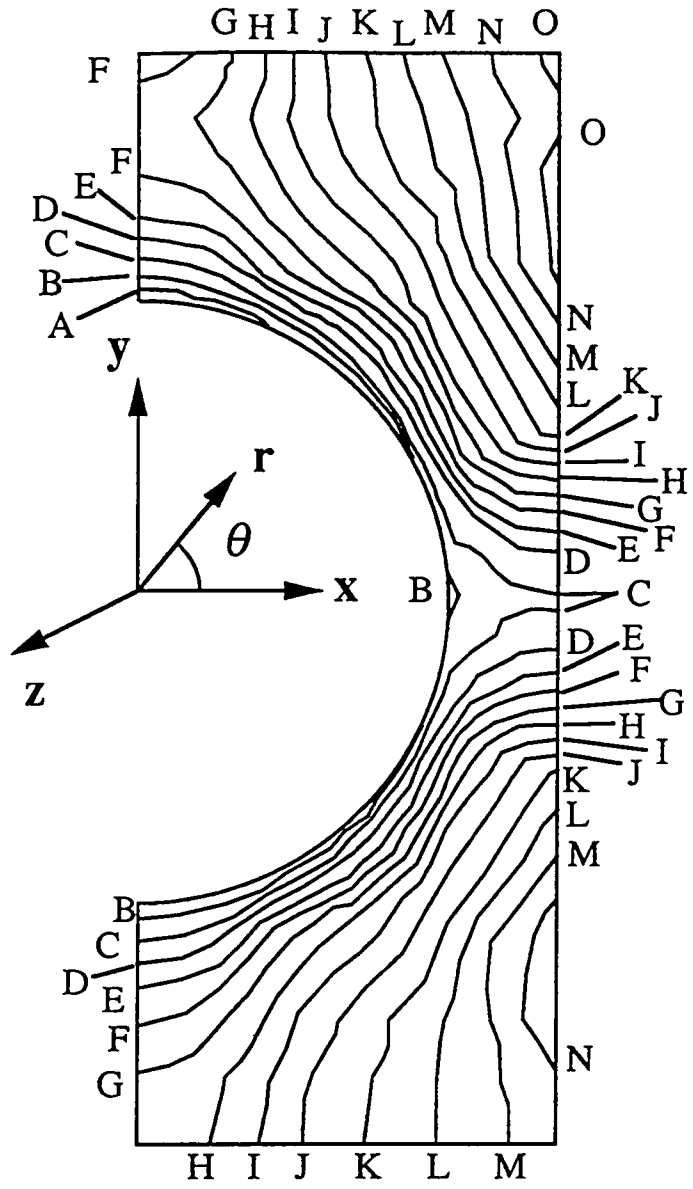

Figure 7. - Matrix $\sigma_{\theta\theta}$ stress contours for two-ply model. Unidirectional SCS-6/Ti-15-3, v_f = 33%, ΔT = -538°C.

Level	Stress (MPa)
A	312
B	296
C	278
D	262
E	245
F	228
G	212
H	195
I	178
J	161
K	144
L	128
M	111
N	94.0
O	77.2

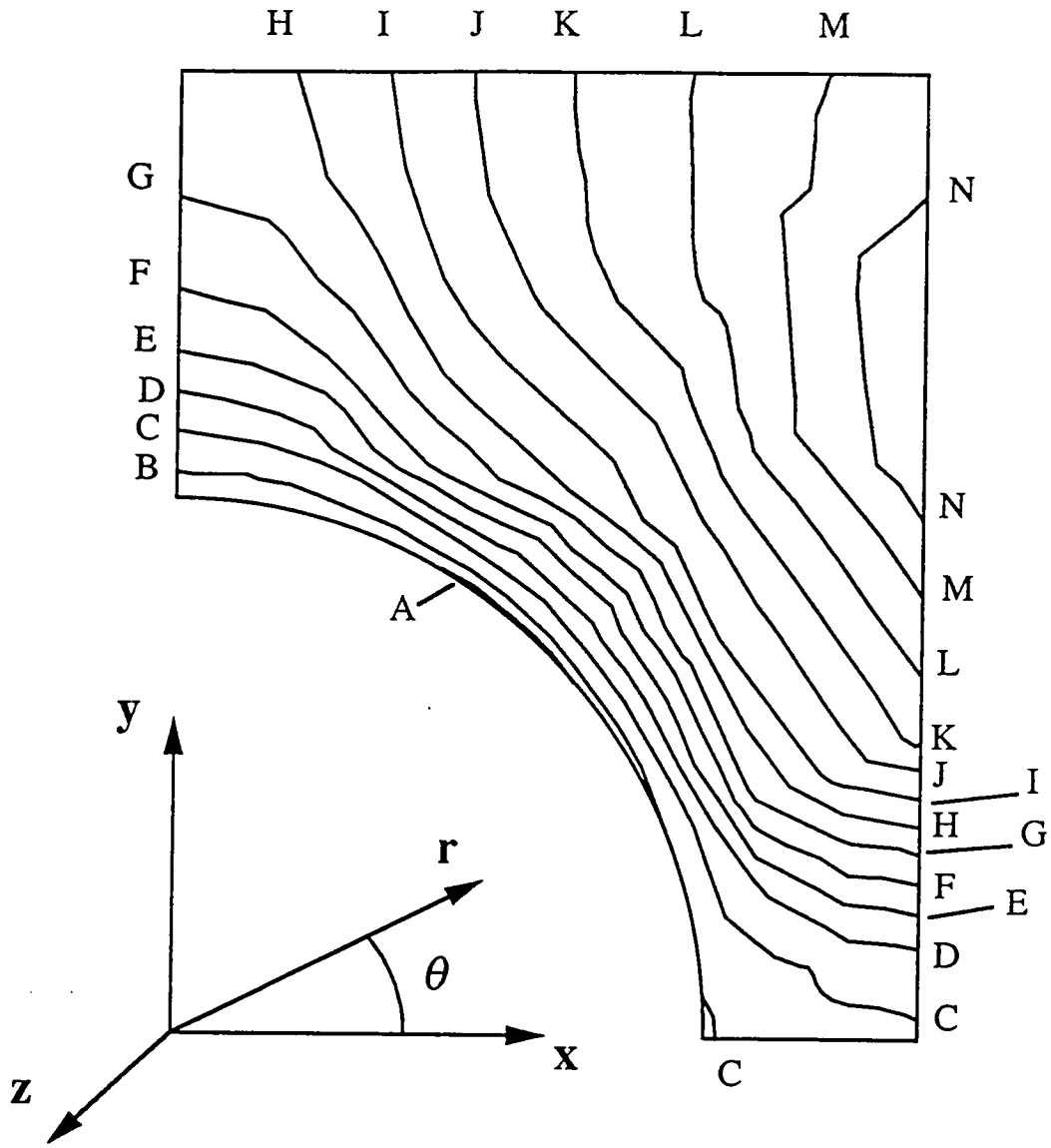

Figure 8. - Matrix $\sigma_{\theta\theta}$ stress contours for infinite array model. Unidirectional SCS-6/Ti-15-3, v_f = 33%, ΔT = -538°C.

Level	Stress (MPa)
A	260
B	255
C	250
D	245
E	240
F	235
G	230
H	225
I	220
J	215
K	210
L	205
M	200
N	195
O	190

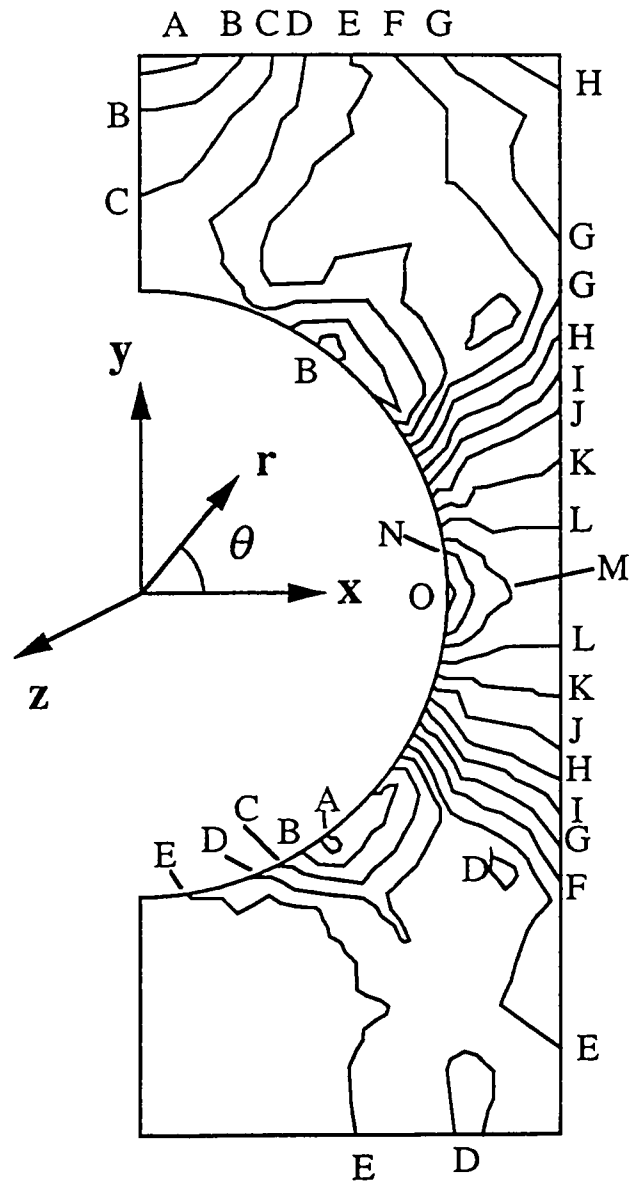

Figure 9. - Matrix σ_{zz} stress contours for two-ply model. Unidirectional SCS-6/Ti-15-3, v_f = 33%, ΔT = -538°C.

Level	Stress (MPa)
A	260
B	255
C	250
D	245
E	240
F	235
G	230
H	225
I	220
J	215
K	210
L	205
M	200
N	195
O	190

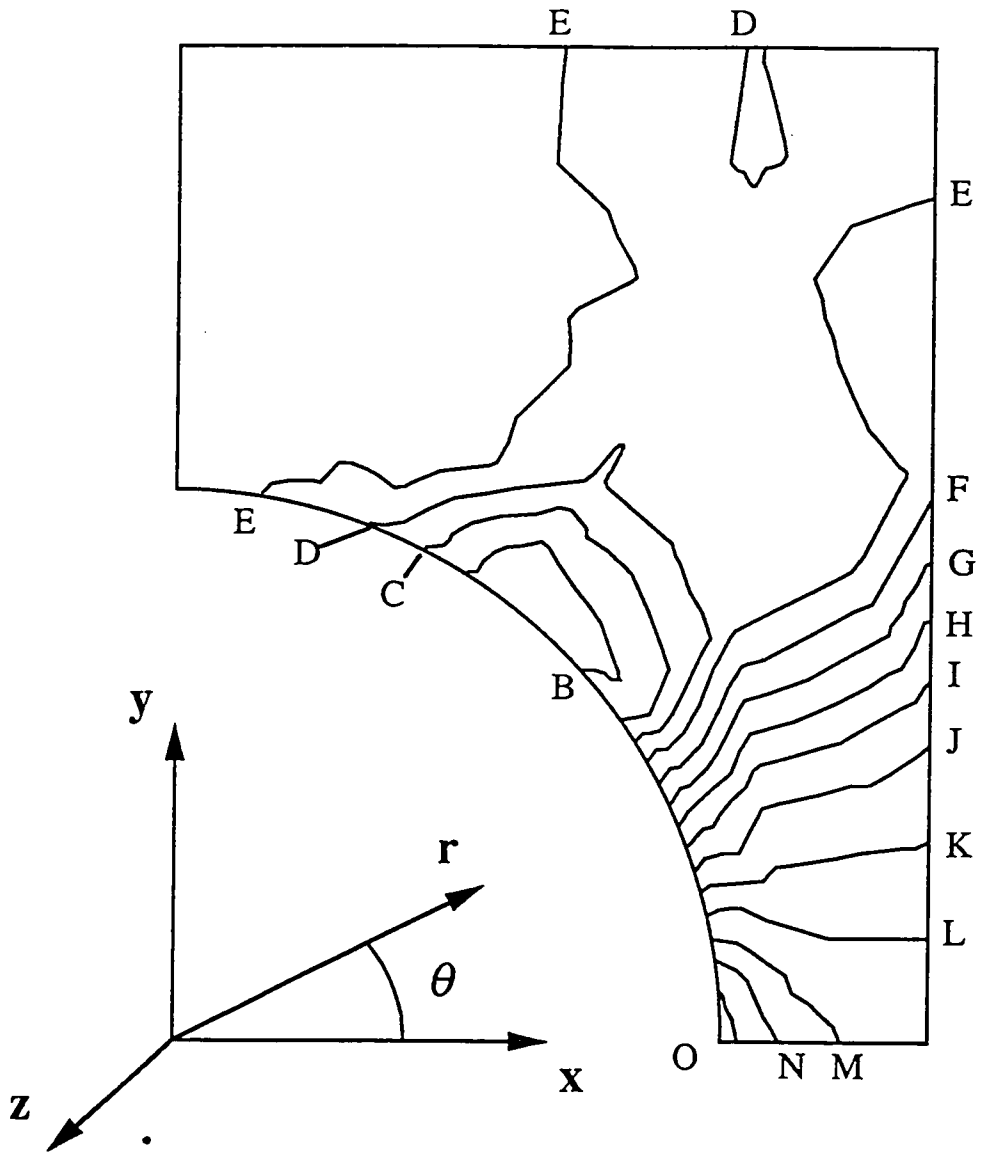

Figure 10. - Matrix σ_{zz} stress contours for infinite array model. Unidirectional SCS-6/Ti-15-3, v_f = 33%, ΔT = -538°C.

Level	Stress (MPa)
A	70.8
B	26.7
C	-17.5
D	-61.6
E	-106
F	-150
G	-194
H	-238

(a) Uniform spacing ($S_1 = S_2 = 0.052$ mm)

Level	Stress (MPa)
A	75.0
B	21.9
C	-31.1
D	-84.2
E	-137
F	-190
G	-243
H	-296

(b) Spacing one ($S_1 = 0.042$ mm)

Level	Stress (MPa)
A	83.7
B	17.5
C	-48.8
D	-115
E	-181
F	-248
G	-314
H	-380

(c) Spacing two ($S_1 = 0.032$ mm)

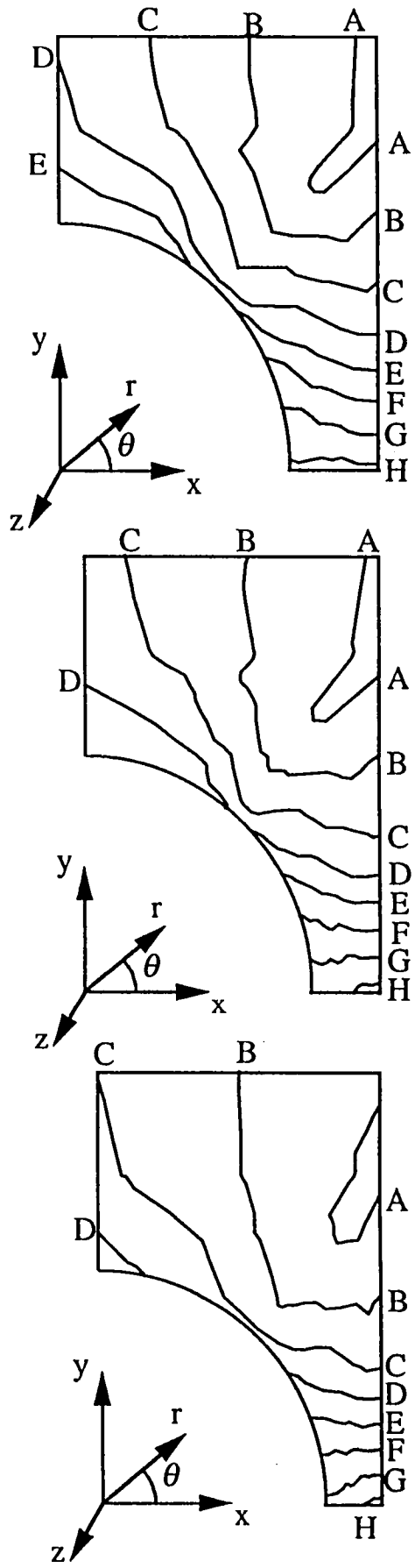

Figure 11. - Matrix σ_{rr} stress contours for interior ply. Unidirectional SCS-6/Ti-15-3, v_f = 33%, $\Delta T = -538^{o}C$.

Level	Stress (MPa)
A	87.6
B	5.27
C	-77.1
D	-159
E	-242
F	-324
G	-406
H	-489

(d) Spacing three (S_1= 0.022 mm)

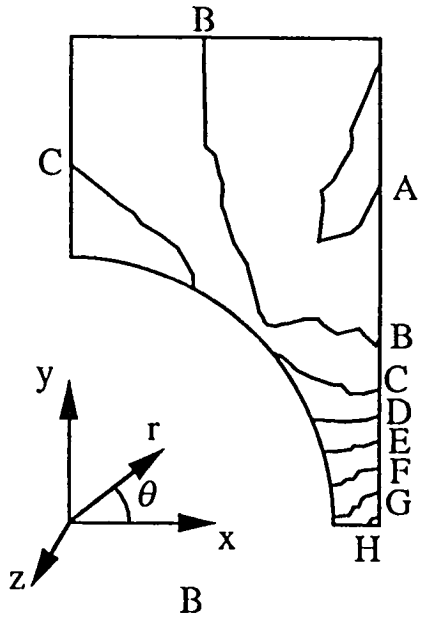

Level	Stress (MPa)
A	97.2
B	-5.83
C	-109
D	-212
E	-315
F	-418
G	-521
H	-624

(e) Spacing four (S_1= 0.012 mm)

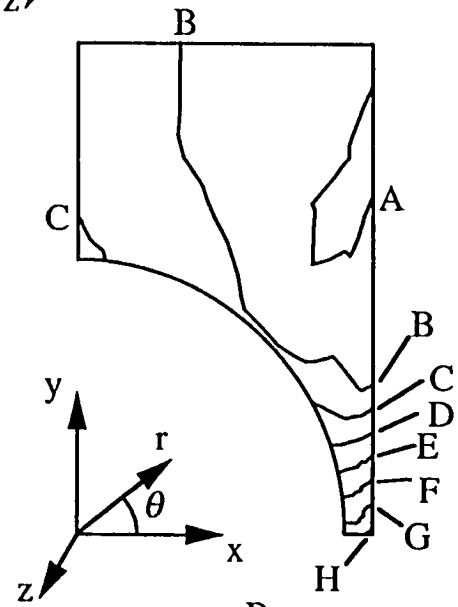

Level	Stress (MPa)
A	121
B	29.3
C	-62.0
D	-153
E	-245
F	-336
G	-427
H	-519

(f) Touching (S_1= 0.0 mm)

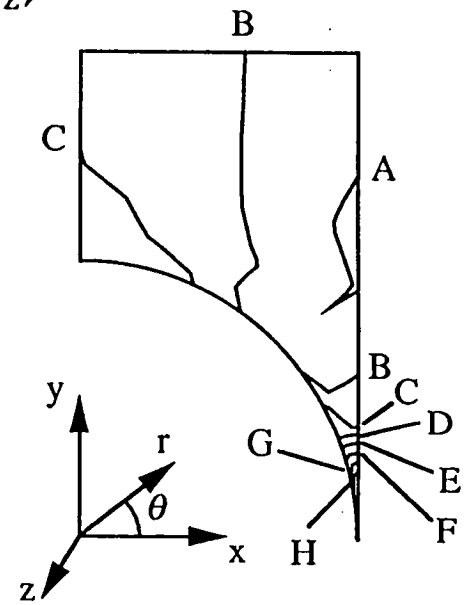

Figure 11. - Continued.

Level	Stress (MPa)
A	287
B	265
C	243
D	221
E	198
F	176
G	154
H	131

(a) Uniform spacing ($S_1 = S_2 = 0.052$ mm)

Level	Stress (MPa)
A	291
B	270
C	248
D	227
E	206
F	184
G	163
H	141

(b) Spacing one ($S_1 = 0.042$ mm)

Level	Stress (MPa)
A	300
B	278
C	256
D	235
E	213
F	191
G	169
H	148

(c) Spacing two ($S_1 = 0.032$ mm)

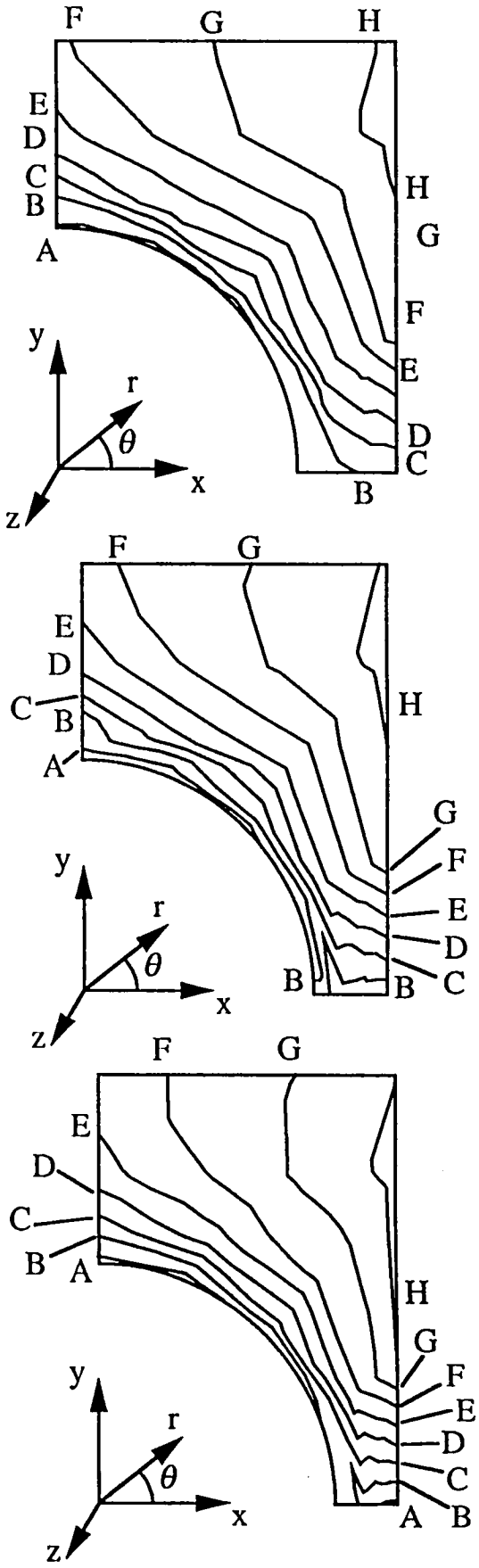

Figure 12. - Matrix $\sigma_{\theta\theta}$ stress contours for interior ply. Unidirectional SCS-6/Ti-15-3, v_f = 33%, ΔT = -538°C.

Level	Stress (MPa)
A	310
B	287
C	265
D	243
E	221
F	199
G	177
H	155

(d) Spacing three (S_1= 0.022 mm)

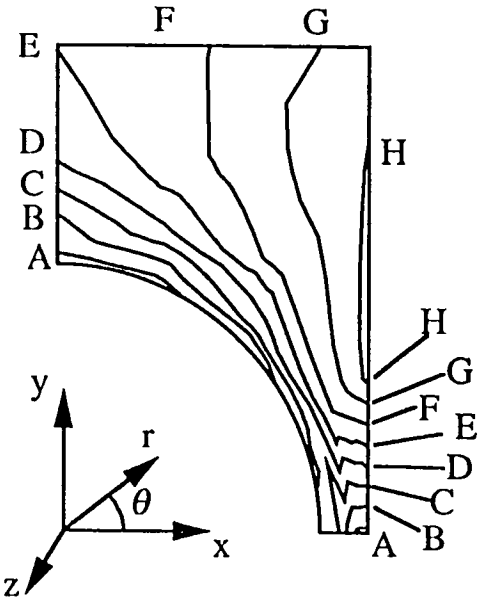

Level	Stress (MPa)
A	317
B	294
C	271
D	249
E	226
F	204
G	181
H	158

(e) Spacing four (S_1= 0.012 mm)

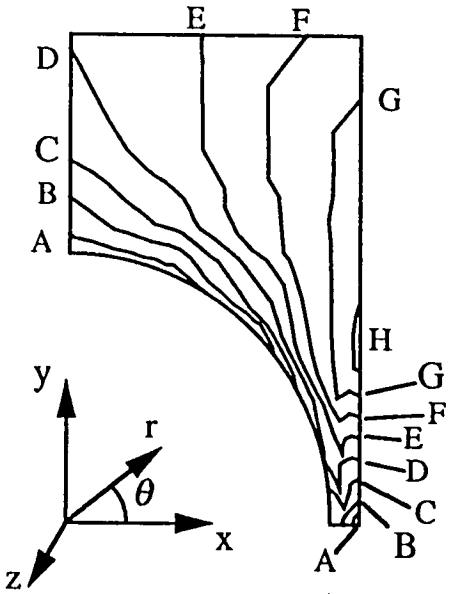

Level	Stress (MPa)
A	485
B	442
C	399
D	356
E	312
F	269
G	226
H	183

(f) Touching (S_1= 0.0 mm)

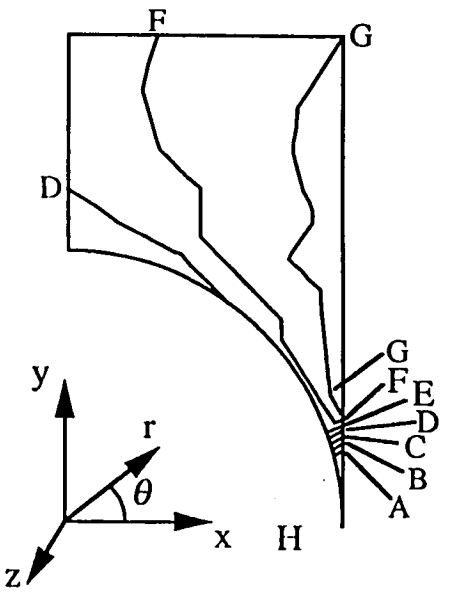

Figure 12. - Continued.

Level	Stress (MPa)
A	260
B	250
C	239
D	228
E	218
F	207
G	196
H	187

(a) Uniform spacing ($S_1 = S_2 = 0.052$ mm)

Level	Stress (MPa)
A	270
B	256
C	250
D	243
E	230
F	217
G	190
H	177

(b) Spacing one ($S_1 = 0.042$ mm)

Level	Stress (MPa)
A	278
B	261
C	244
D	227
E	210
F	193
G	175
H	158

(c) Spacing two ($S_1 = 0.032$ mm)

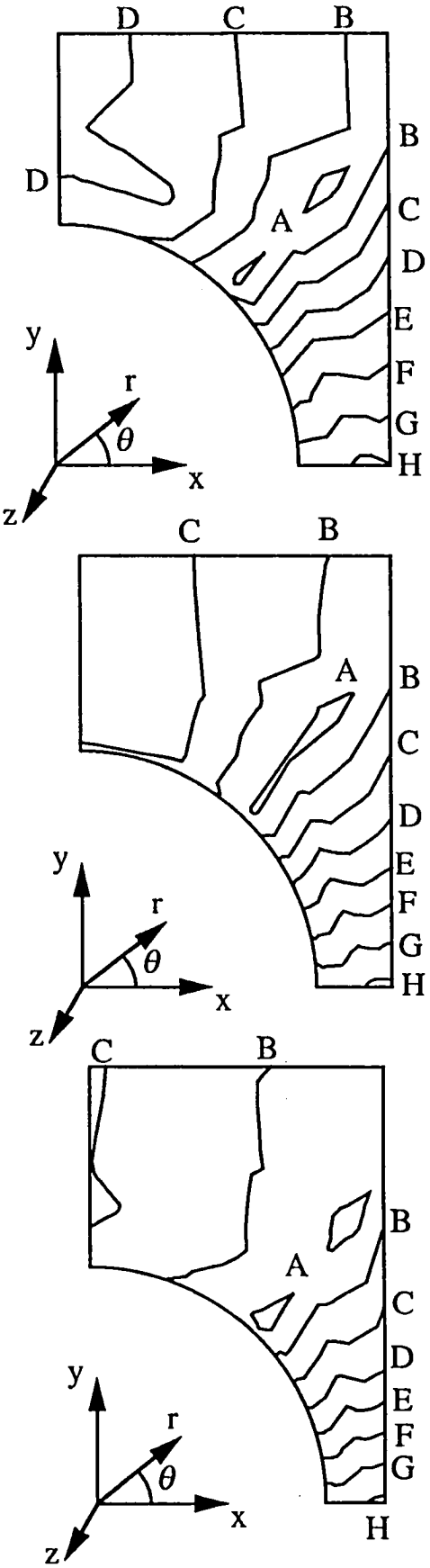

Figure 13. - Matrix σ_{zz} stress contours for interior ply. Unidirectional SCS-6/Ti-15-3, v_f = 33%, ΔT = -538°C.

Level	Stress (MPa)
A	287
B	265
C	242
D	219
E	197
F	174
G	152
H	129

(d) Spacing three (S_1 = 0.022 mm)

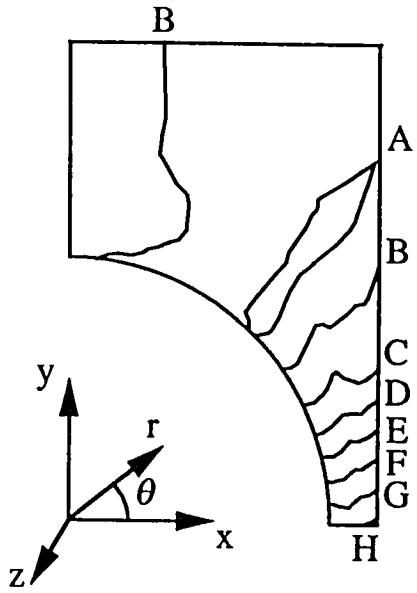

Level	Stress (MPa)
A	301
B	270
C	238
D	206
E	174
F	143
G	111
H	79.4

(e) Spacing four (S_1 = 0.012 mm)

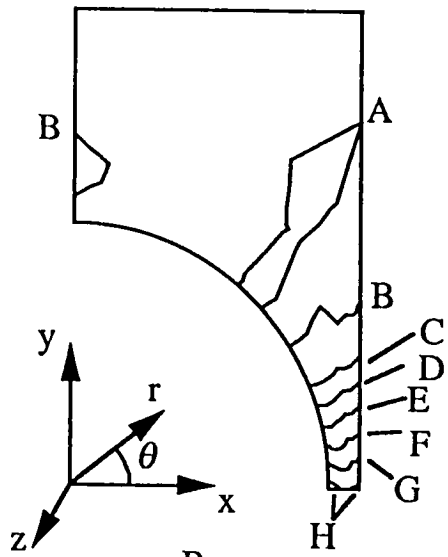

Level	Stress (MPa)
A	339
B	302
C	265
D	229
E	192
F	155
G	118
H	81.6

(f) Touching (S_1 = 0.0 mm)

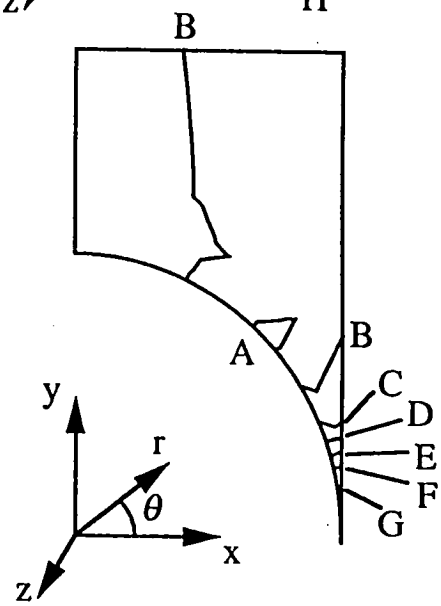

Figure 13. - Continued.

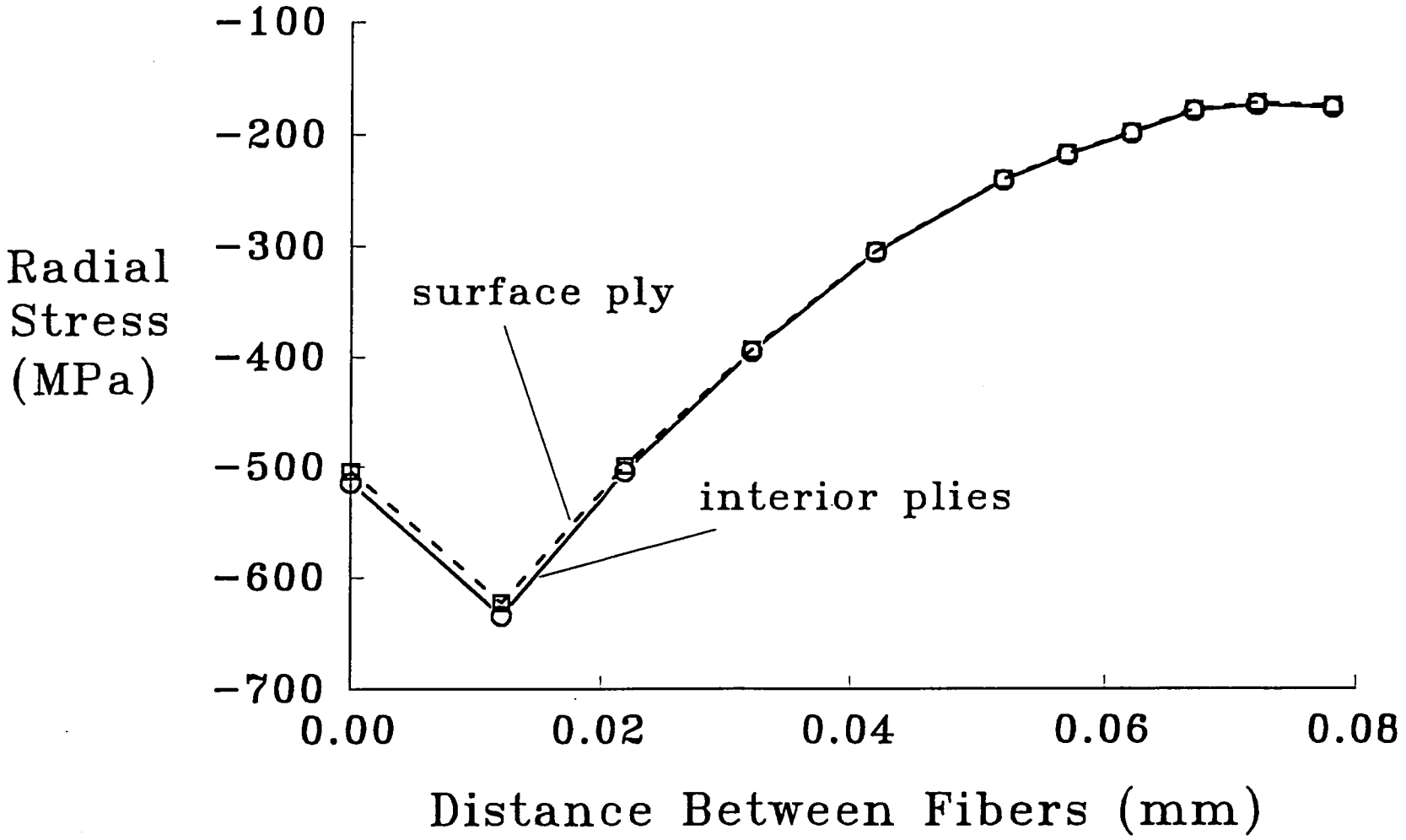

Figure 14. - Maximum σ_{rr} stress in the matrix. Unidirectional SCS-6/Ti-15-3, v_f = 33%, ΔT = -538°C.

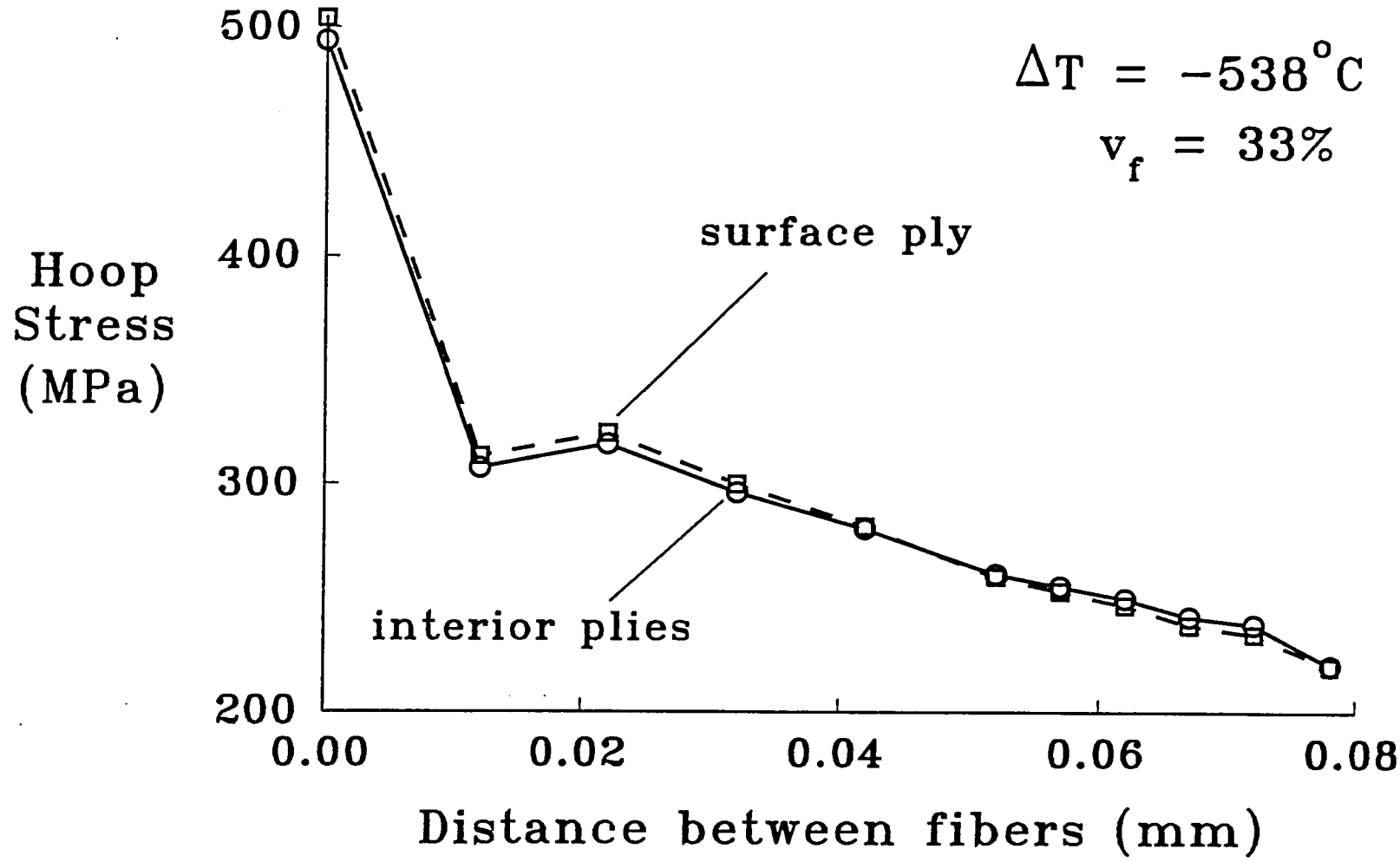

Figure 15. - Maximum $\sigma_{\theta\theta}$ stress in the matrix. Unidirectional SCS-6/Ti-15-3, v_f = 33%, ΔT = -538°C.

fig18

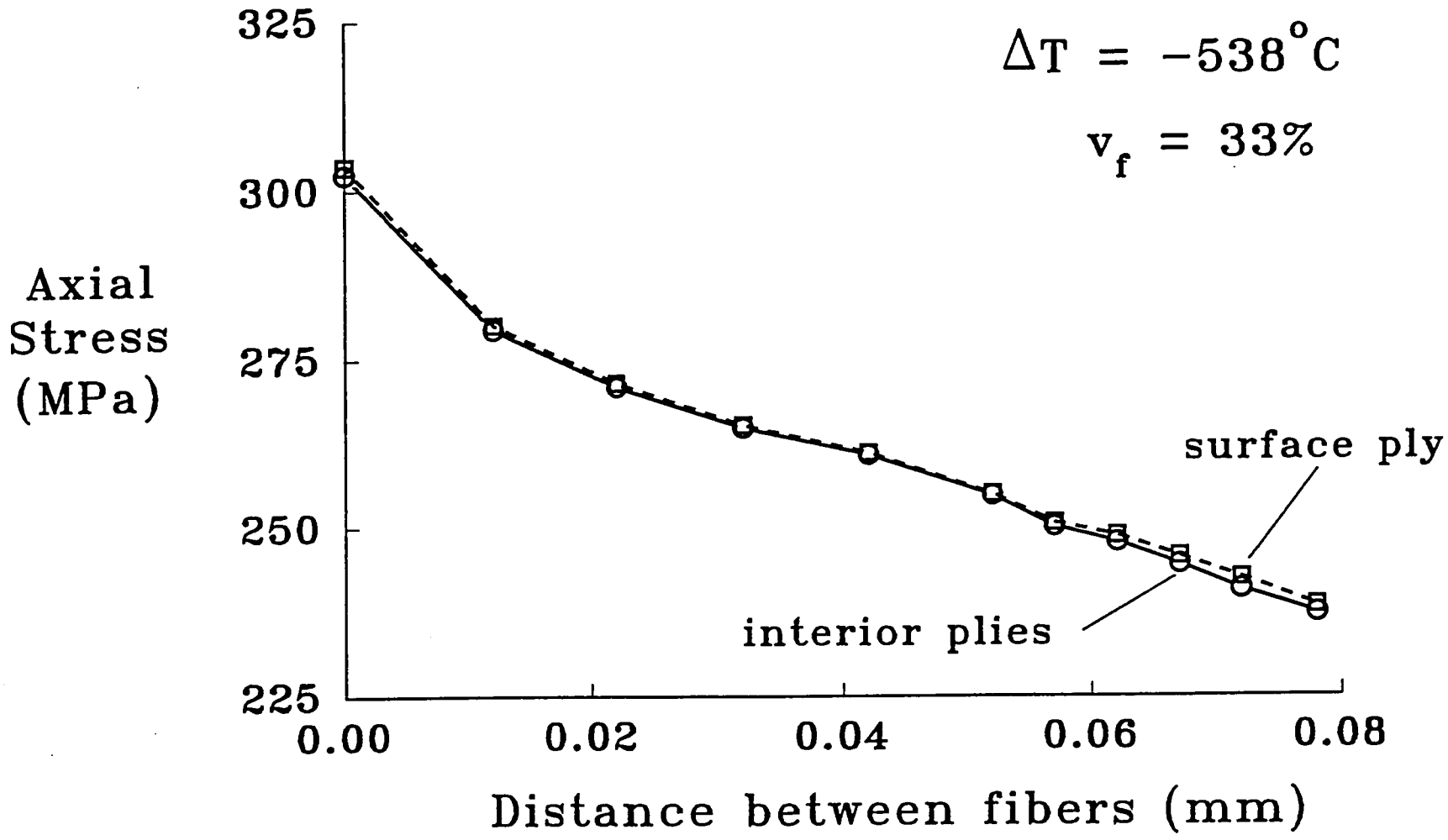

Figure 16. - Maximum σ_{zz} stress in the matrix. Unidirectional SCS-6/Ti-15-3, v_f = 33%, ΔT = -538°C.

fig19

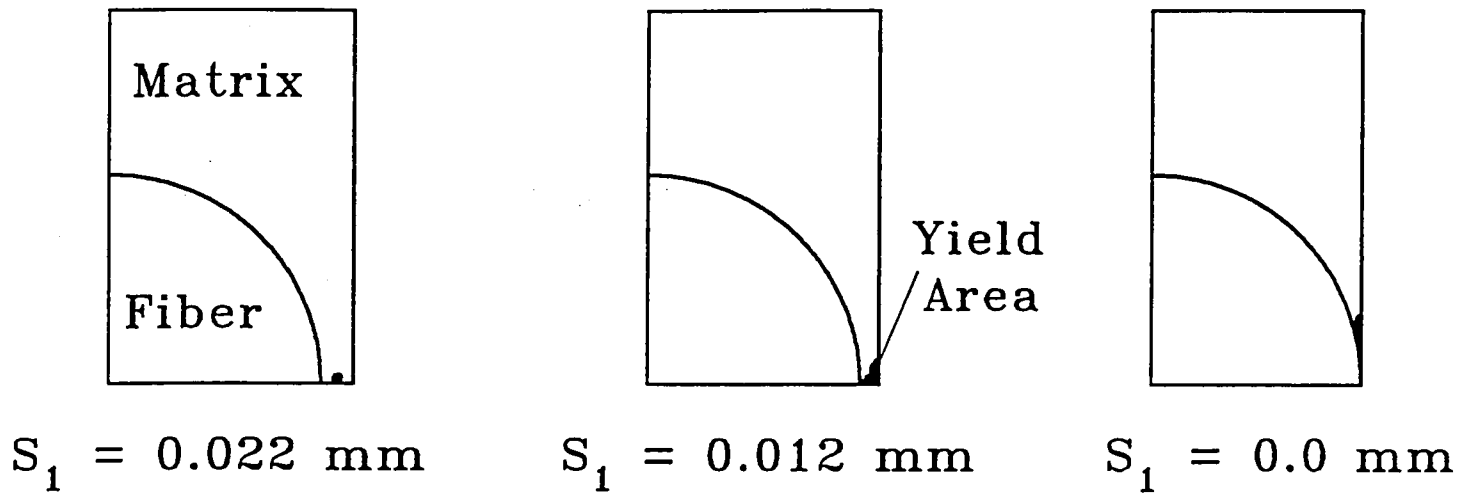

Figure 17. - Matrix yielding for interior plies. Unidirectional SCS-6/Ti-15-3, v_f = 33%, ΔT = -538°C.

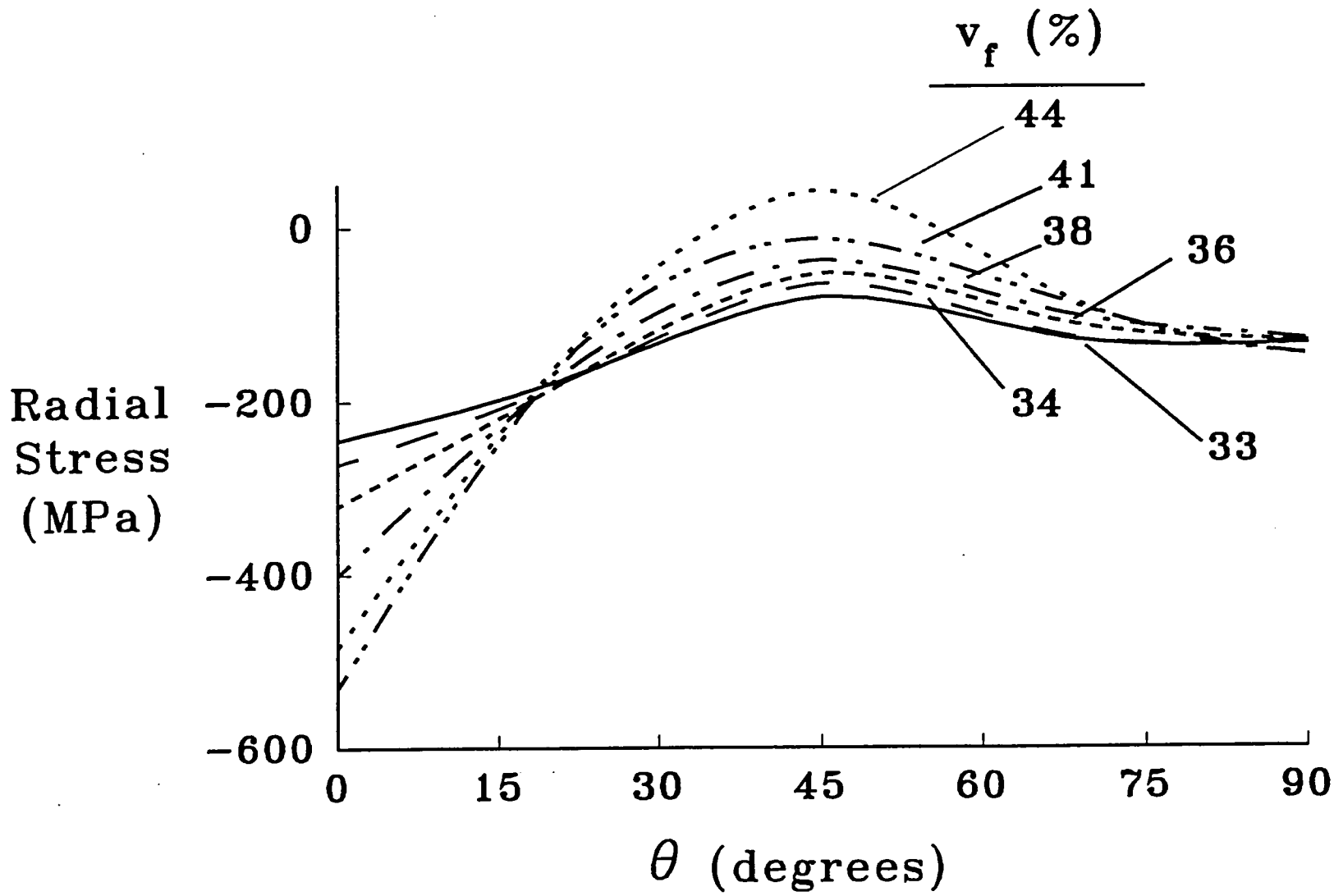

Figure 18. - Matrix σ_{rr} stresses at fiber-matrix interface for various fiber volume fractions. Unidirectional SCS-6/Ti-15-3, $\Delta T = -538^{o}C$.

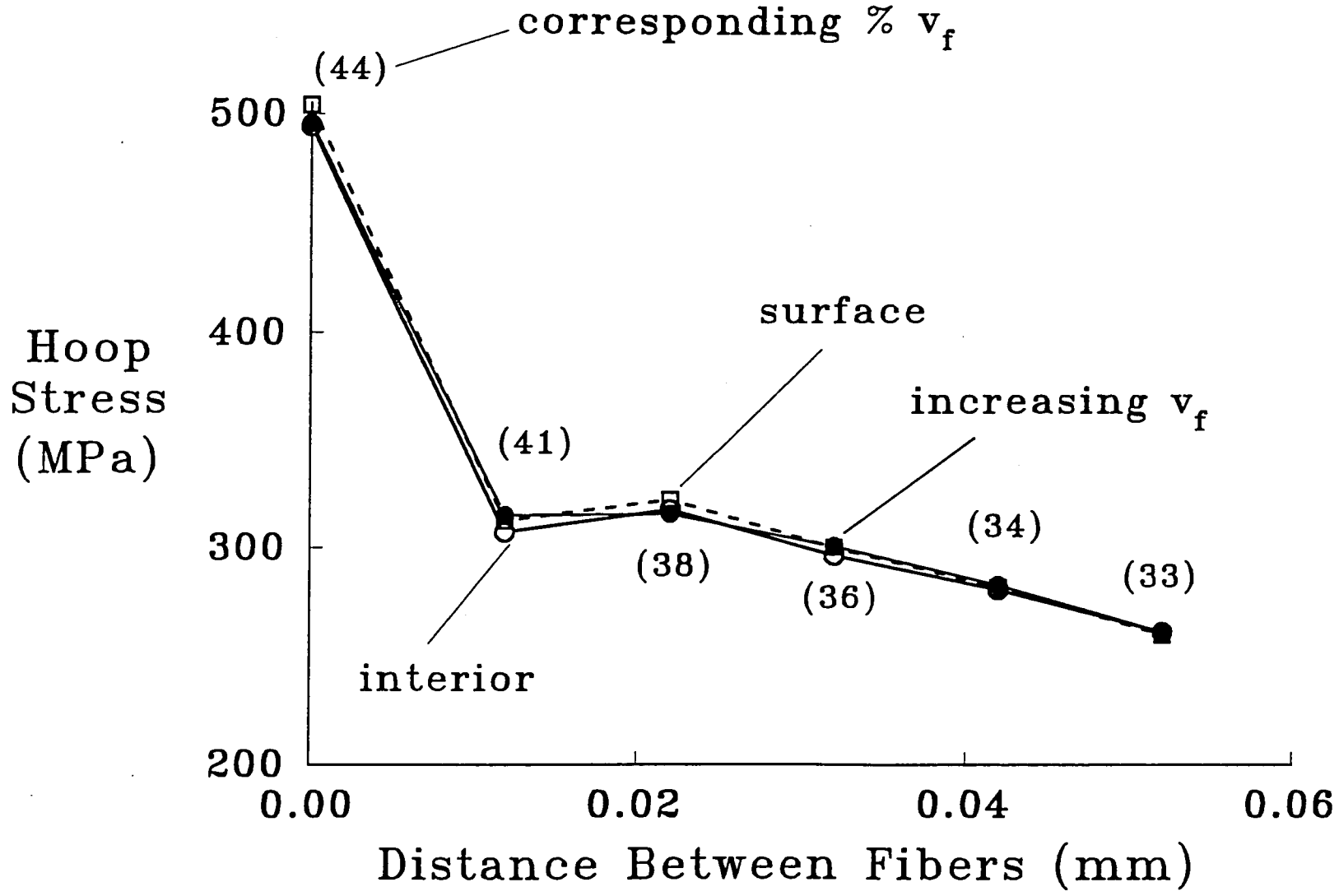

Figure 19. - Matrix $\sigma_{\theta\theta}$ stress for various fiber volume fractions. Unidirectional SCS-6/Ti-15-3, $\Delta T = -538^{o}C$.

figvf

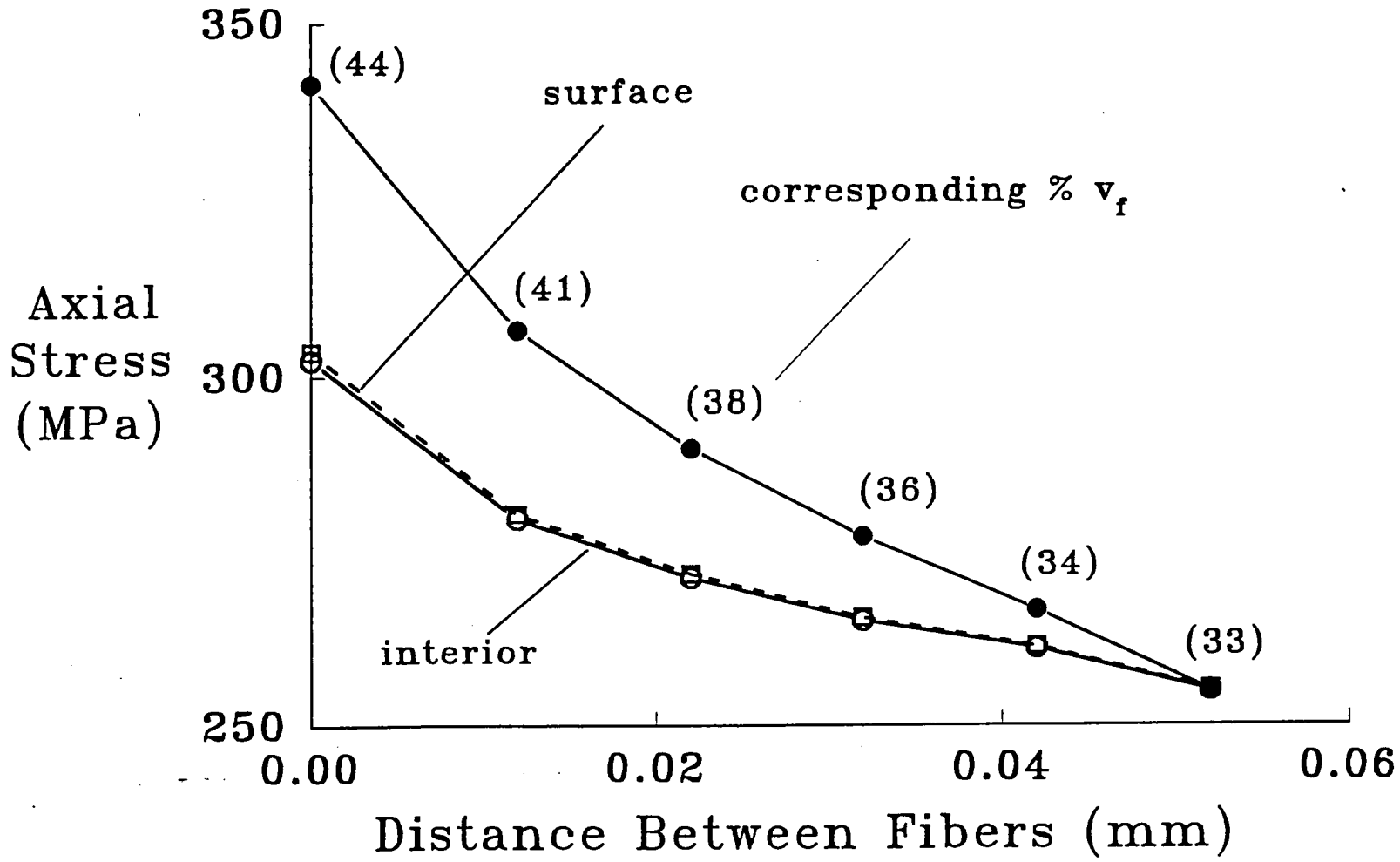

Figure 20. - Maximum σ_{zz} matrix stress for various fiber volume fractions. Unidirectional SCS-6/Ti-15-3, $\Delta T = -538^{o}C$.

axialvf

REPORT DOCUMENTATION PAGE

Form Approved
OMB No. 0704-0188

1. AGENCY USE ONLY (Leave blank)	2. REPORT DATE	3. REPORT TYPE AND DATES COVERED
	March 1992	Technical Memorandum

4. TITLE AND SUBTITLE

The Effects of Uneven Fiber Spacing on Thermal Residual Stresses in a Unidirectional SCS-6/Ti-15-3 Laminate

5. FUNDING NUMBERS

WU 763-23-41

6. AUTHOR(S)

C. A. Bigelow

7. PERFORMING ORGANIZATION NAME(S) AND ADDRESS(ES)

NASA Langley Research Center
Hampton, VA 23665-5225

8. PERFORMING ORGANIZATION REPORT NUMBER

9. SPONSORING/MONITORING AGENCY NAME(S) AND ADDRESS(ES)

National Aeronautics and Space Administration
Washington, DC 20546

10. SPONSORING/MONITORING AGENCY REPORT NUMBER

NASA TM-104225

11. SUPPLEMENTARY NOTES

12a. DISTRIBUTION/AVAILABILITY STATEMENT

Unclassified - Unlimited

Subject Category 24

12b. DISTRIBUTION CODE

13. ABSTRACT *(Maximum 200 words)*

High residual stresses develop in SCS-6/Ti-15-3 composites during cooldown from the fabrication temperature; these residual stresses can effect the mechanical and physical properties of the composite. Discrete fiber-matrix finite element models were used to study the residual stresses due to the temperature change during the fabrication process, including the effects of uneven fiber spacing, the free surface, and increased fiber volume fractions.

To accurately model the effects of the free surface, it is only necessary to model one fiber through the thickness. Below the first ply, the analysis predicts stress distributions that are identical to the infinite array predictions.

For uneven fiber spacing less than 0.042 mm in an interior ply, the maximum hoop stress was predicted to occur between fibers within a ply and increased as the fiber spacing decreased. The maximum hoop stress correlated well with the observed radial cracking between fibers. For the case of touching fibers, the analysis predicted tensile radial stresses at the fiber-matrix interface, which could lead to fiber-matrix debonding during the fabrication cooldown. Identical trends were predicted for uneven fiber spacing in surface plies with slightly greater values of maximum stresses.
The analysis predicted matrix yielding to occur upon cooldown when the edge-to-edge fiber spacing was less than or equal to 0.022 mm. The stress distributions predicted for increasing fiber volume fractions were similar to those predicted for decreasing the fiber spacing for two adjacent fibers within a ply.

14. SUBJECT TERMS

Free surface; Fiber volume fraction; Micromechanics; Matrix cracks; Finite elements

15. NUMBER OF PAGES

45

16. PRICE CODE

A03

17. SECURITY CLASSIFICATION OF REPORT	18. SECURITY CLASSIFICATION OF THIS PAGE	19. SECURITY CLASSIFICATION OF ABSTRACT	20. LIMITATION OF ABSTRACT
Unclassified	Unclassified		